CORA Cork Open Research Archive
Cartlann Taighde Oscailte Chorcaí

Title	Optical spectroscopy for biological and biomedical applications: potentially impacting future of healthcare with research, clinical translation and education
Authors	Saito Nogueira, Marcelo
Publication date	2021-11-10
Original Citation	Saito Nogueira, M. 2021. Optical spectroscopy for biological and biomedical applications: potentially impacting future of healthcare with research, clinical translation and education. PhD Thesis, University College Cork.
Type of publication	Doctoral thesis
Rights	© 2021, Marcelo Saito Nogueira. - https://creativecommons.org/licenses/by-nc-sa/4.0/
Download date	2026-11-17 11:25:36
Item downloaded from	https://hdl.handle.net/10468/14150

UCC
University College Cork, Ireland
Coláiste na hOllscoile Corcaigh

Chapter 5

Effect of optical properties in light distribution

Marcelo Saito Nogueira

This chapter is part of the thesis "Optical spectroscopy for biological and biomedical applications: potentially impacting future of healthcare with research, clinical translation and education" by Marcelo Saito Nogueira

The rest of the thesis can be accessed via CORA UCC:

cora.ucc.ie

Please ensure appropriate acknowledgement and referencing when using material and/or ideas outlined in this thesis.

Contents

5. Effect of optical properties in light distribution 171
5.1 Elastic and inelastic scattering processes 171
5.2 Absorption processes 177
5.3 Luminescence processes 180
5.4 Convolution of light beams with finite spatial and temporal widths 181
5.5 Implications on modeling light behavior in reflectance and transmittance geometries 185
5.6 References 186

5. Effect of optical properties in light distribution

Once the mathematical description of light propagation models is clear to the reader, chapter 5 builds up the intuition on concepts related to the temporal and spatial light distribution based on optical properties of biological media such as tissues, biofluids and biosolids. However, the relationship between the mathematical formulation of these concepts and the graphical representation of experimentally-related quantities is missing and is required to understand the modeling of light propagation in biological media. In this chapter, a comprehensive guide on such concepts is shown by associating (1) optical processes, (2) semi-quantitative medium light distribution profiles, and (3) quantitative temporal and spatial profiles of light intensity. Explanations and schematic drawings illustrate the light behavior upon shining infinitesimally narrow light beams ("pencil" beams) on the medium, or upon shining light beams with finite spatial and temporal widths on it. Light distribution concepts of chapter 5 can be directly used for optical treatments in aesthetics, tattoo/port-whine stain removal, laser surgeries, and any other application which requires treatment planning based on effects of light in the targeted medium (e.g., heating for photothermal therapy, spatially- and time-resolved efficiency of generation of singlet oxygen and reactive oxygen species for photodynamic therapy, and others) [1–121–3,5–12]. Applications requiring a detector need to take into account light propagation from the source and detectors, which will be mainly covered in chapter 6.

5.1 Elastic and inelastic scattering processes

As per previous chapters, the effects of light propagation in complex media can be associated with the fundamental optical processes depending on the medium optical properties (e.g., refractive index, light absorption, luminescence and (elastic or inelastic) scattering, Table 4.1). Hence, predicting measured quantities at different illumination configurations as well as light collection over a certain area (or probing a specific volume in the medium) requires understanding of the impact of optical properties in the light distribution. The easiest way to understand this impact is visually relating the spatial and temporal light distribution with the fundamental optical processes upon variation of medium optical properties.

Figure 5.1 shows a schematic drawing of the spatial distribution of the light along with detectable reflected light at each distance from the light source positioned at the end of the arrow pointing downwards. This distribution is shown for semi-infinite homogeneous medium geometry as the most common geometry for optical tomography, imaging and point spectroscopy. More light represented by darker colors. If we assume radial geometry in this case, one can observe the cross-section of a cylinder and represent the light distribution in cylindrical coordinates. Hence, fluence rates and the intensity of (subdiffuse or diffuse) reflected light can be described as a function of radius r. For simplicity, we can consider monitoring the behavior of diffuse light which can be modeled by equations of Chapter 4. In this case, steady state fluence rates can be calculated by using the equation derived in section 4.10.2 and the intensity can be calculated by integrating the exiting light at the surface area of the detector at a given position r. Then, the intensity of excitation light decays radially as it propagates through the medium. Since this intensity depends on the integration of the fluence rate at the detector area, it is important to note that this intensity is zero at the source position (detector area = 0). This intensity is also dependent on the area of light source and, therefore, a convolution must be performed by considering this area, as explained in more detail in subsequent figures of this chapter.

When modeling the diffuse reflected light as a function of time (figure 5.2), the light propagation occurs similarly to what is represented in figure 4.8 (following the absorption, dilution and spatial diffusion wave factors), but with boundary conditions of a semi-infinite medium. In this case, the reflected light is only detected after the time of scattering events (at least two) experienced by light before it exits the medium.

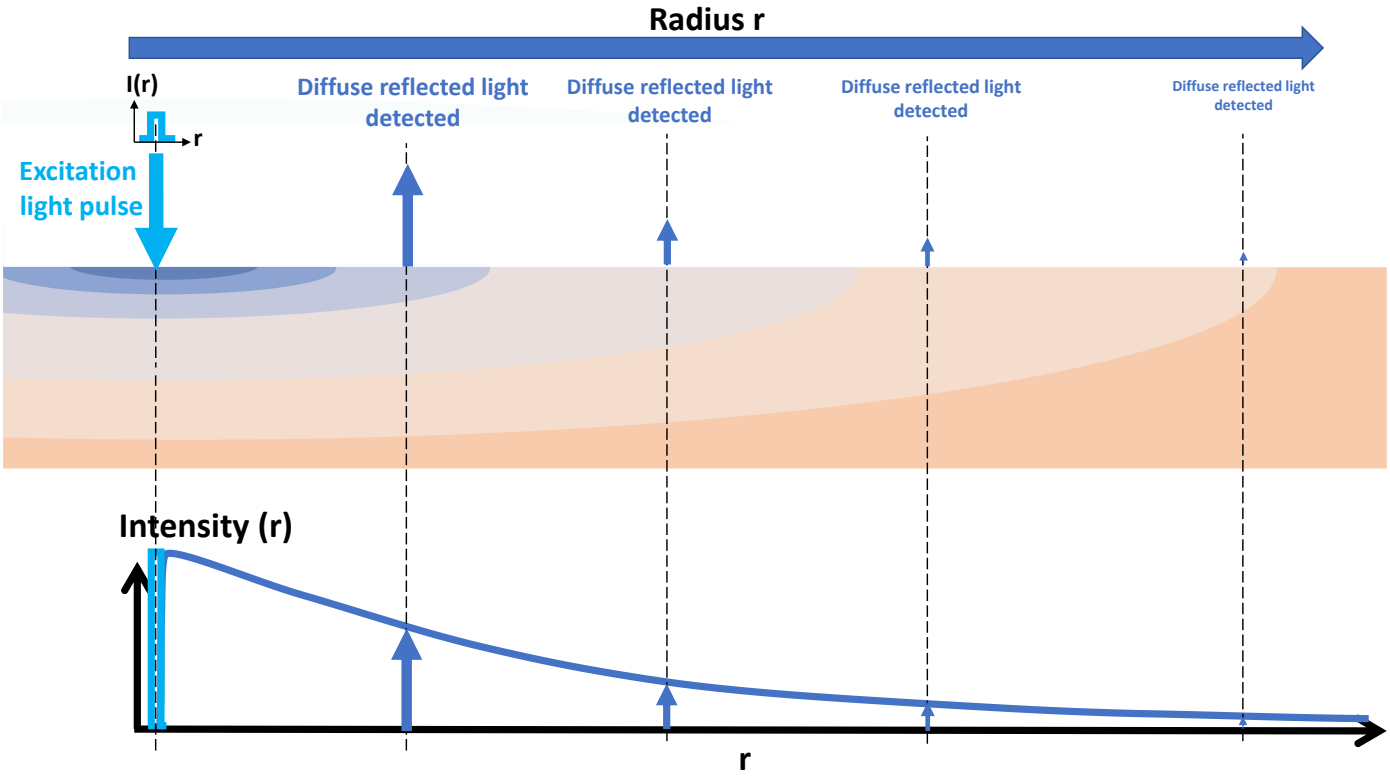


Figure 5.1: Spatial light distribution and diffuse reflected light intensity in a scattering medium upon illumination by a finite-sized light beam.

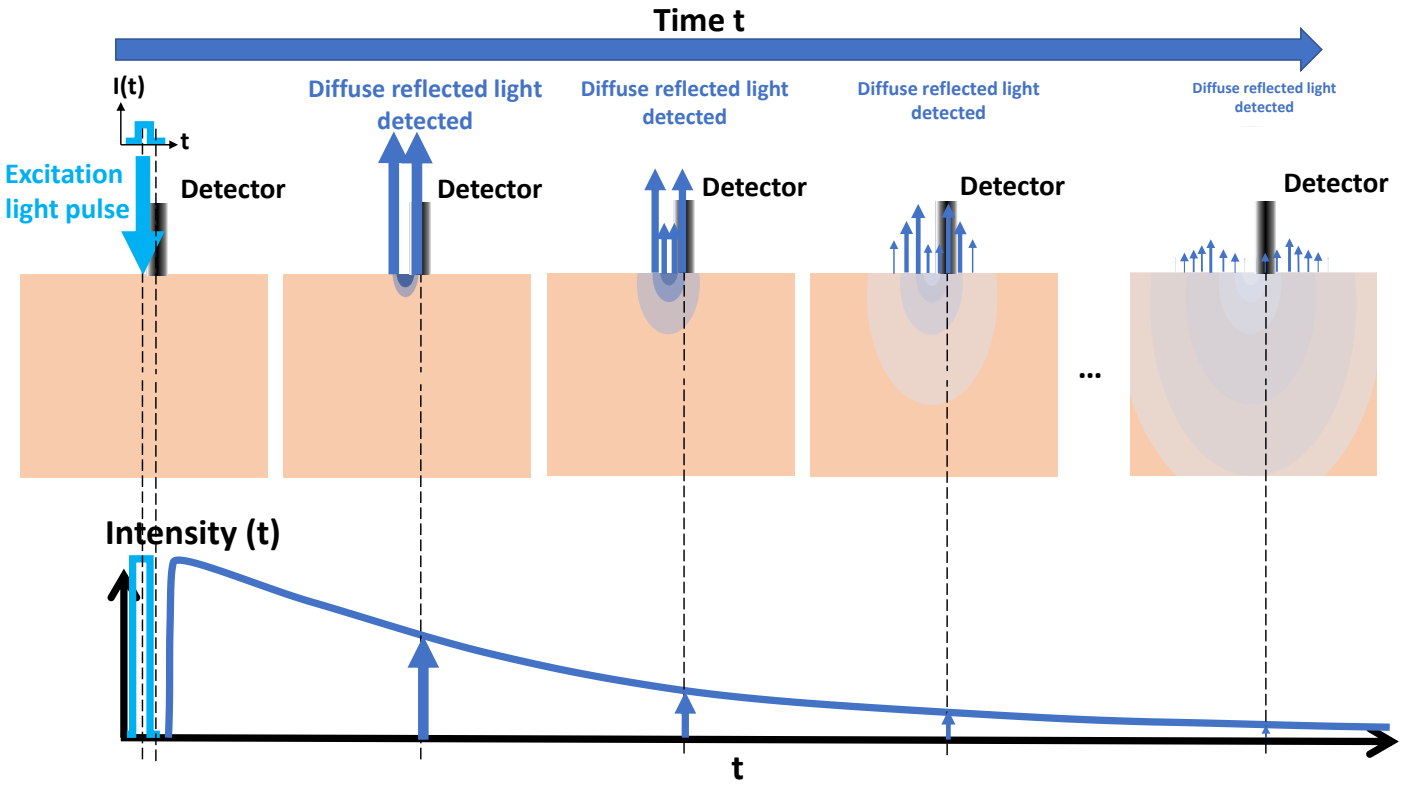


Figure 5.2: Temporal evolution of light distribution and the diffuse reflected light (detected at a fixed position) in a scattering medium upon illumination by a short pulse of light with finite width.

It is worth noting that the behaviors of spatial and temporal light distributions are inter-related (figures 5.1 and 5.2), as light traveling over larger distances takes more time to propagate and vice-versa. With this in mind, we cover the principles of the spatial distribution which are easier to be visualized in static figures (and tend to be more intuitive and

well-received by most audiences) and which can be translated to the temporal distribution in the medium (whose visualization would require videos or sequence of frames).

The spatial distribution of light intensity (or fluence rate) is strongly associated with the probability of photon absorption and scattering. Increased scattering coefficient while maintaining a constant anisotropy factor (equivalent to increase in reduced scattering coefficient, figure 5.3) leads to less light propagation in the direction of incidence (perpendicularly to the medium surface) and to photons exiting through the medium surface at shorter distances from the light source. The change in light propagation and exitance can be visualized by the behavior of photons traveling over longer distances within the medium, as illustrated in figure 5.3 by equivalent photon paths in lower or higher scattering media. Figure 5.3 shows that the larger the medium μ_s' , the shorter distances diffuse reflected photons exit at in the medium surface where light enters the medium and the longer distances diffuse transmitted photons exit through the opposite surface.

The behavior of light propagation can be fundamentally associated to the higher probability of changing the direction of propagation at larger μ_s' values, which results in:

- Higher light attenuation in the radial direction.
- Higher fluence rates spatially close to the light source.
- The thicker the medium, the lower the transmitted intensity (incidence direction - dashed line).
- The shorter the distance from the light source, the higher the detected reflected intensity.

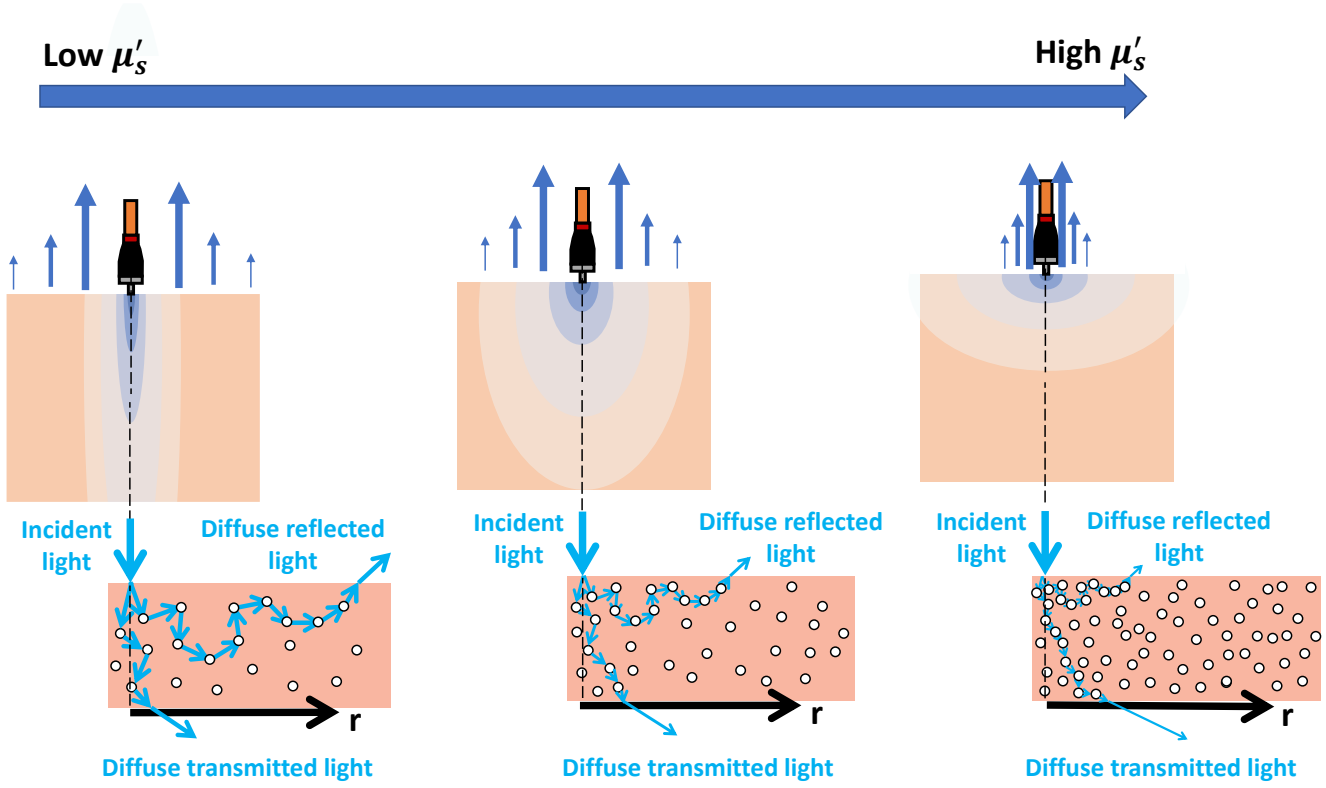


Figure 5.3: Schematic of the relationship between spatial light distribution and light propagation in scattering media with increasing μ_s' values upon illumination by an infinitesimally narrow light beam (point source).

The aforementioned results can be translated to the temporal behavior of light distribution (figure 5.4) and propagation (detection at a fixed distance from the light source), in which larger μ_s' leads to (refer to figure 5.4):

- Higher light attenuation (fewer surviving photons) for longer propagation times.
- Photon distribution over longer periods of time (light pulse broadening).
- The larger the propagation time, the lower the detected light intensity (less probability of late photons to be found within the medium without exiting its surface).
- Less photons detected at shorter times after the light pulse (less early photons).

The effects described above occur due to the light dilution as photons scatter throughout the medium (dilution factor) and as light exits the medium at a distance r from the light source position r_s, similarly to what has been described by the components of the time-resolved diffusion equation obtained in section 4.10.1 for infinite homogeneous medium geometry, but for a semi-infinite medium geometry. These effects result in the spatial and temporal light distribution illustrated in figures 5.4 (elastic scattering) and 5.5 (inelastic scattering). Figure 5.4 schematically shows the spatial-resolved (i.e., radial-resolved at the medium surface) and temporal-resolved intensities in reflectance geometry upon excitation by a narrow light beam or short pulse of light, respectively. By visualizing the propagation of a late-photon at scattering media, once can see the radial distance (r axis) where most photons already exited the medium through its surface (i.e., where most photons were diffuse reflected). This distance is indicated by the dashed line of figure 5.4.

In semi-infinite (purely) scattering media, no photon is transmitted through the medium. Since no light is transmitted, the number of incident photons equals to the total number of diffuse reflected photons. This number can be calculated by the integration of light intensity over the entire tissue surface. Figure 5.4 shows the spatial (radial) intensity profile for the same input light intensity. As it be seen from the figure, the conservation of the number of photons leads to the aforementioned behavior of larger number of photons exiting the surface at shorter distances from the source, which means more light would be detected at settings with source-to-detector distances (SDD) for larger μ_s' values.

Even though figure 5.4 represents the behavior of spatially-resolved reflected intensity as μ_s' varies and either decreased μ_s or increased anisotropy factors g cause photons to take larger distances (travel through larger pathlengths) to come back to the surface, it is worth remembering that this intensity the shape of the light distribution is changed differently upon variation of μ_s or g factor (chapter 4, section 4.1.2 Absorption and scattering properties, figure 4.4). Hence, the curvature of the exponential decay of the reflected intensity will depend on both μ_s and g.

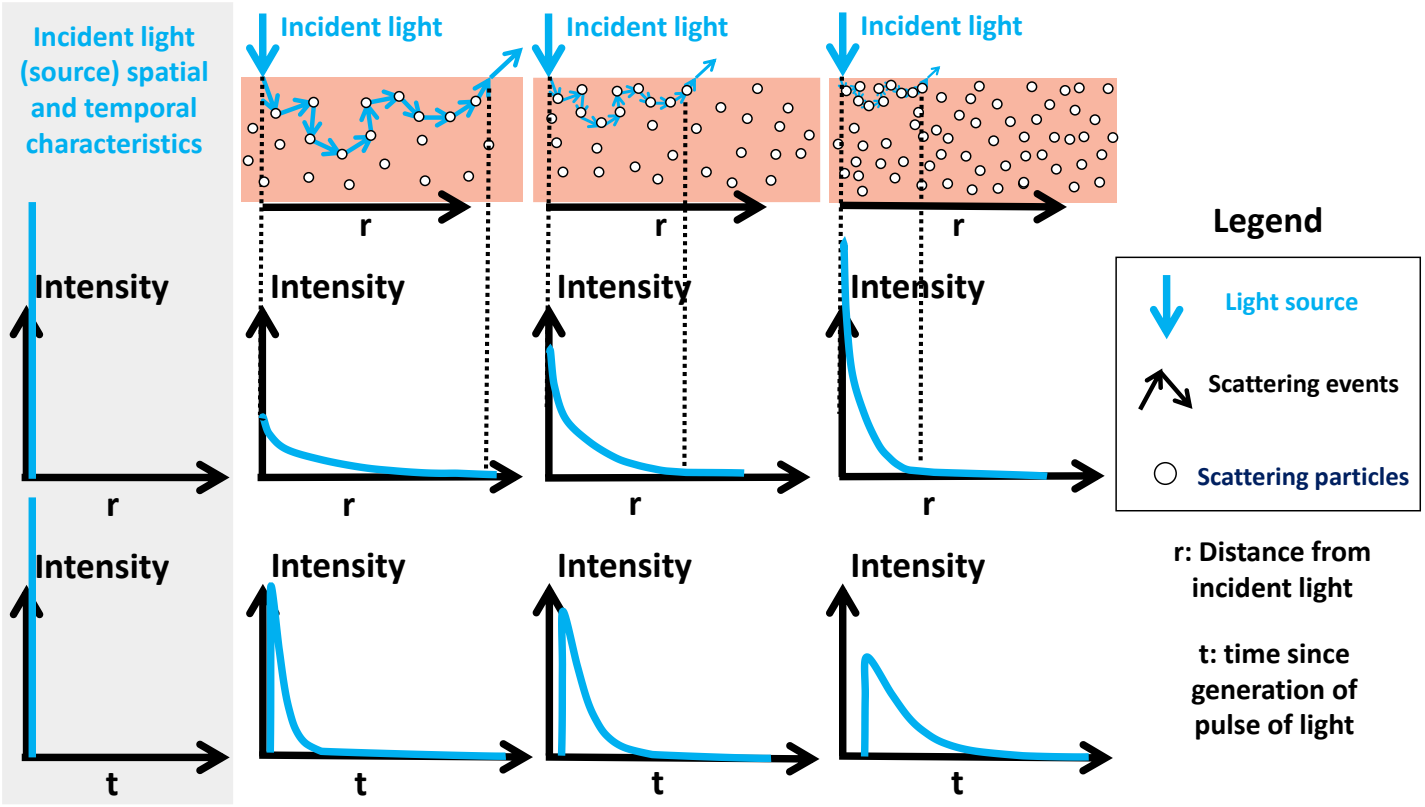


Figure 5.4: Schematic of the relationship between light propagation and diffuse reflected intensity as a function of radial distance r from an infinitesimally narrow light beam (point source) and as a function of time t (for a fixed position in the medium) in scattering media with increasing μ_s' values. Schematics of intensity graphs are shown in linear scale. The dashed lines indicate the position of the light source and the distance where most photons exited the scattering medium.

Regarding the temporal behavior of diffuse reflected light following excitation by a short pulse of light, one can see that the light pulse becomes broader and more shifted towards larger time stamps once the medium μ_s' increases. A similar behavior as increasing μ_s' is expected when the pulse of light travels over larger distances such as for increasing tissue thicknesses in transmittance measurements, as both pulse broadening and shift depend on the number of scattering events within the medium.

The spatial and temporal distribution of inelastic scattered light follows the same behavior as the elastic scattered light phenomenologically. The main difference between the two types of scattering processes is the dimension of the Raman scattering coefficient μ_{Raman}, which is typically ~10^{-7} times lower than μ_s' values of biological tissues [13], as described in chapter 4. Since Raman scattering is typically treated as a single scattering process but the probability of Raman scattering still increases with μ_{Raman} (defining the Raman scattering cross section) and the local light flux (increased by μ_s' for shorter distances from the source), I chose to show the behavior of Raman scattering in a multiple scattering media with fixed μ_s' and increasing μ_{Raman} (figure 5.5; increasing μ_{Raman} linearly increases the amplitude of the diffuse Raman reflected intensity, but does not change the spatial and time intensity decays) and multiple scattering media with increasing μ_s' and fixed μ_{Raman} (figure 5.6; equivalent to the case where μ_{Raman} is sufficient large to cause Raman multiple scattering). However, if the concentration of Raman scattering particles is sufficient large to cause multiple Raman scattering, the behavior of the diffuse Raman reflected intensity is analogous to the multiple scattering regime of Mie scattered light shown previously in figure 5.4. In addition, it is important to remember that the anisotropy of Raman scattering is still not well defined, as characterizing the anisotropy of the extensive list of sources of Raman scattered light can be challenging, as numerous vibrational modes contribute to the Raman signal in biological media [14,15] (chapter 7, section 7.2 Sources of Raman scattering in biological media). Furthermore, although this signal is generated

by vibrational modes of specific molecular bonds, the signal is also affected by the microenvironment of molecules generating the Raman signal, which generates a high degree of complexity in obtaining Raman anisotropy factors for Raman scatterers.

Still, it is known that the light propagation / distribution in Raman scattering processes should follow the same behavior as Rayleigh scattering, as both are scattering phenomena happening at similar scales (smaller than wavelength; e.g., at molecular or submolecular scales).

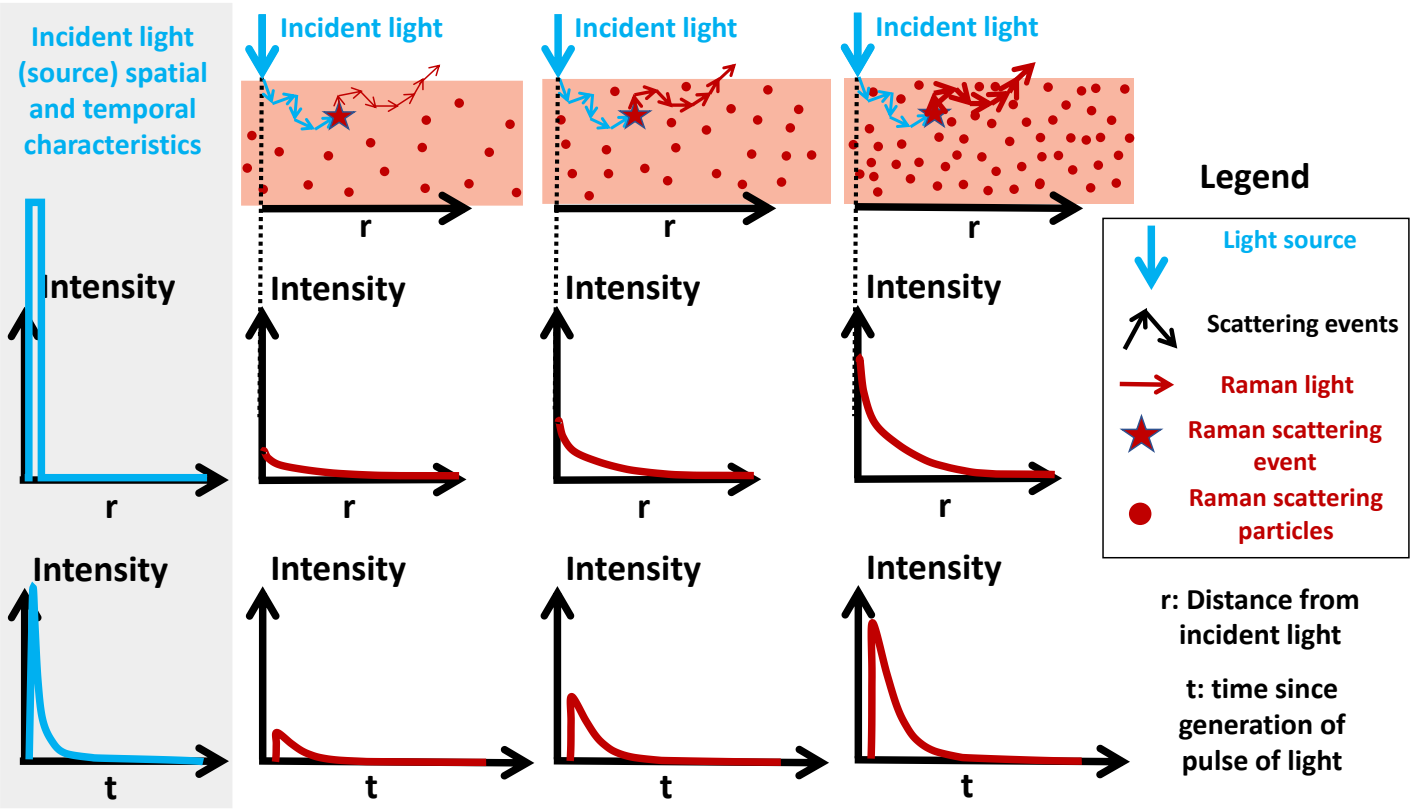


Figure 5.5: Schematic of the relationship between light propagation and diffuse Raman reflected intensity as a function of radial distance r from an infinitesimally narrow light beam (point source) and as a function of time t (for a fixed position in the medium) in scattering media with fixed μ_s' and increasing μ_{Raman}, assuming Raman scattering is a single scattering process. Schematics of intensity graphs are shown in linear scale. increasing μ_{Raman} linearly increases the amplitude of the diffuse Raman reflected intensity, whereas the shape of intensity profile remains the same regardless of the μ_{Raman} of the medium.

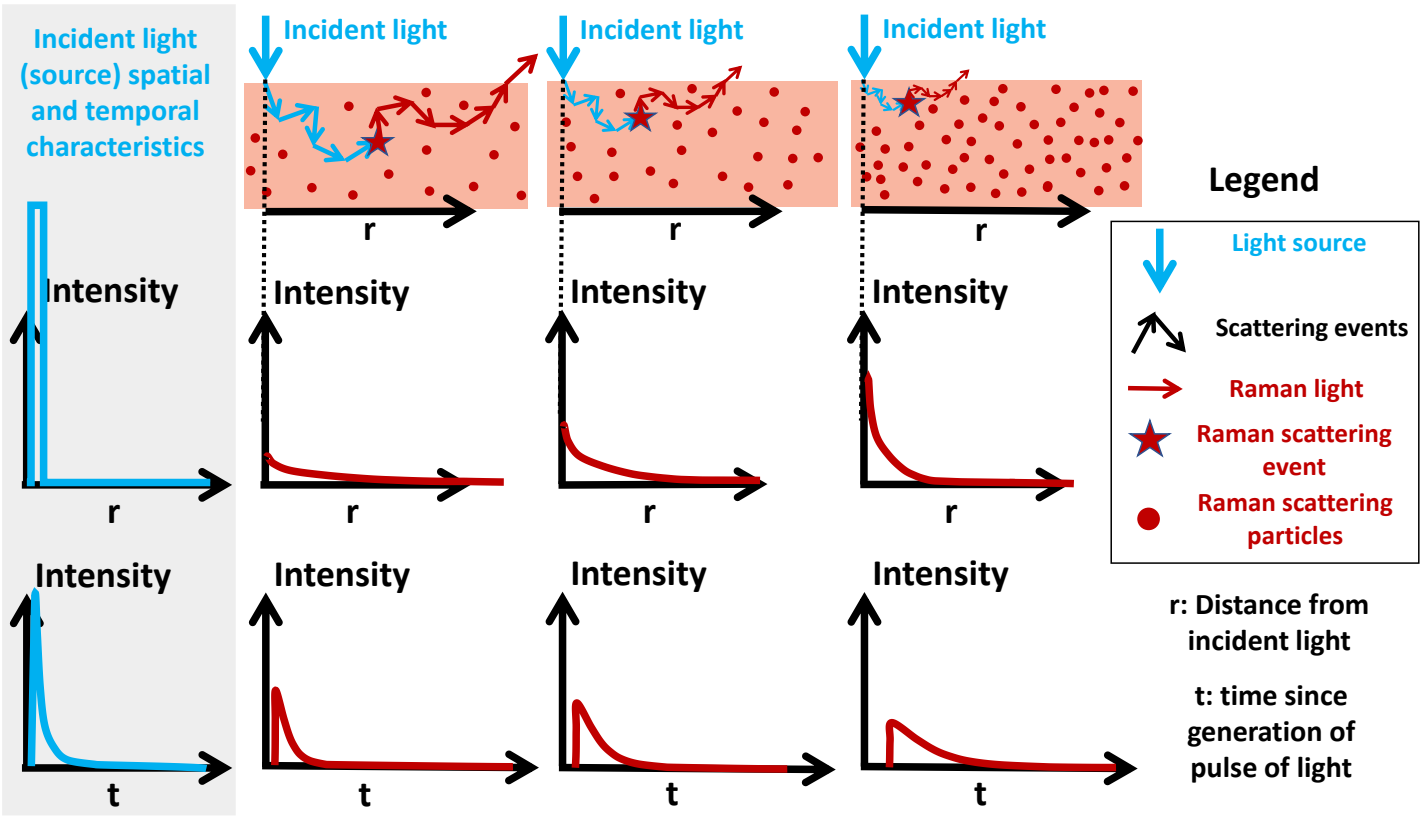


Figure 5.6: Schematic of the relationship between light propagation and diffuse Raman reflected intensity as a function of radial distance r from an infinitesimally narrow light beam (point source) and as a function of time t (for a fixed position in the medium) in scattering media with increasing μ_s' values and containing a fixed concentration of Raman scattering particles (fixed μ_{Raman}) or Raman scattering media with increasing μ_{Raman} values when sufficient number of Raman scattering particles can cause multiple Raman scattering. Schematics of intensity graphs are shown in linear scale. The shape of intensity profile follows the same trends of that multiple scattering media, but with considerably lower intensity due to the much smaller magnitude of Raman scattering cross-section.

5.2 Absorption processes

Absorption processes are simpler to visualize, as they are directly involved in light attenuation. The relationship between the light distribution and its propagation in absorbing media can be envisioned as decreased light intensity due to increased probability of absorption for larger μ_a values, and at longer propagation distances and times. Upon increasing the medium μ_a, light becomes more attenuated in every direction and photons have a lower chance of survival. This attenuation upon larger μ_a values results in:

- Higher light attenuation at all directions within the absorbing medium.
- Higher fluence rates (lower attenuation) spatially close to the light source.
- The thicker the medium, the lower the transmitted intensity (incidence direction - dashed line) due to higher attenuation at larger distances.
- The shorter the distance from the light source, the higher the detected reflected intensity.

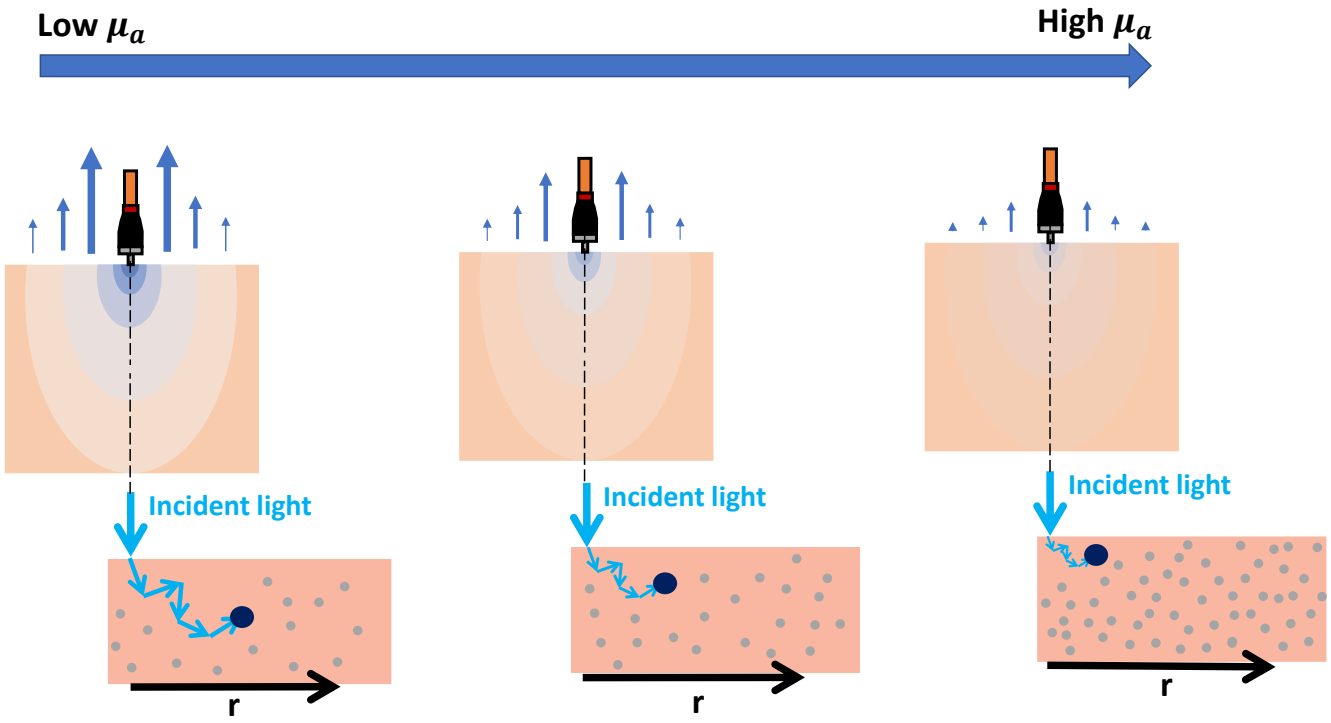


Figure 5.7: Schematic of the relationship between spatial light distribution and light propagation upon illumination by an infinitesimally narrow light beam (point source).

The analogy with the temporal behavior of light propagation (detection at a fixed distance from the light source), in which larger μ_a leads to (refer to figure 5.7):

- Higher light attenuation (fewer surviving photons) for longer propagation times.
- Photon distribution over shorter periods of time (light pulse narrowing).
- The larger the propagation time, the lower the detected light intensity (lower probability of photon survival leading to less late photons).
- Most photons (less than the total input photons) are detected at shorter times after the light pulse (more early photons, as late photons have a lower change of survival).

The effects described above occur due to the light absorption as photons propagate throughout the medium (absorption factor) similarly to what has been described by the components of the time-resolved diffusion equation obtained in section 4.10.1 for infinite homogeneous medium geometry, but for a semi-infinite medium geometry. These effects result in the spatial and temporal distribution of light in absorbing media follows the aforementioned effects of absorption on the probability of photon survival. In purely absorbing media, there is no reflectance and transmittance can be described by the Beer-Lambert law. When scattering is present, diffusion theory may describe changes upon meeting the requirements of its validity (chapter 4, section 4.9 Diffusion equation) and, when the condition $\mu_a \ll \mu_s'$ is not met, light propagation can still be described by using probabilistic methods (chapter 4, section 4.12 Probabilistic methods of light propagation) or modified Beer-lambert law [16,17].

In order to schematically show the light attenuation due to absorption effects, I illustrated the behavior of narrow light beam or short pulse of light following single scattering (figure 5.8) and multiple scattering (figure 5.9) in absorbing and scattering media. In single scattering and absorbing media, the width of the light beam or pulse does not broaden in either space or time and absorption is the predominant effect. In this case, figure 5.8 illustrates the decrease of light intensity as well as the temporal narrowing of the incoming light pulse. Similarly, this decrease and narrowing can be observed in multiple scattering and absorbing media (figure 5.9). The visualization of the propagation of a late-photons in these media evidence the radial distance (r axis) where most photons have been absorbed, as indicated by the dashed

line. As expected, the higher the absorption, the shorter distances and times the light propagates within the complex medium.

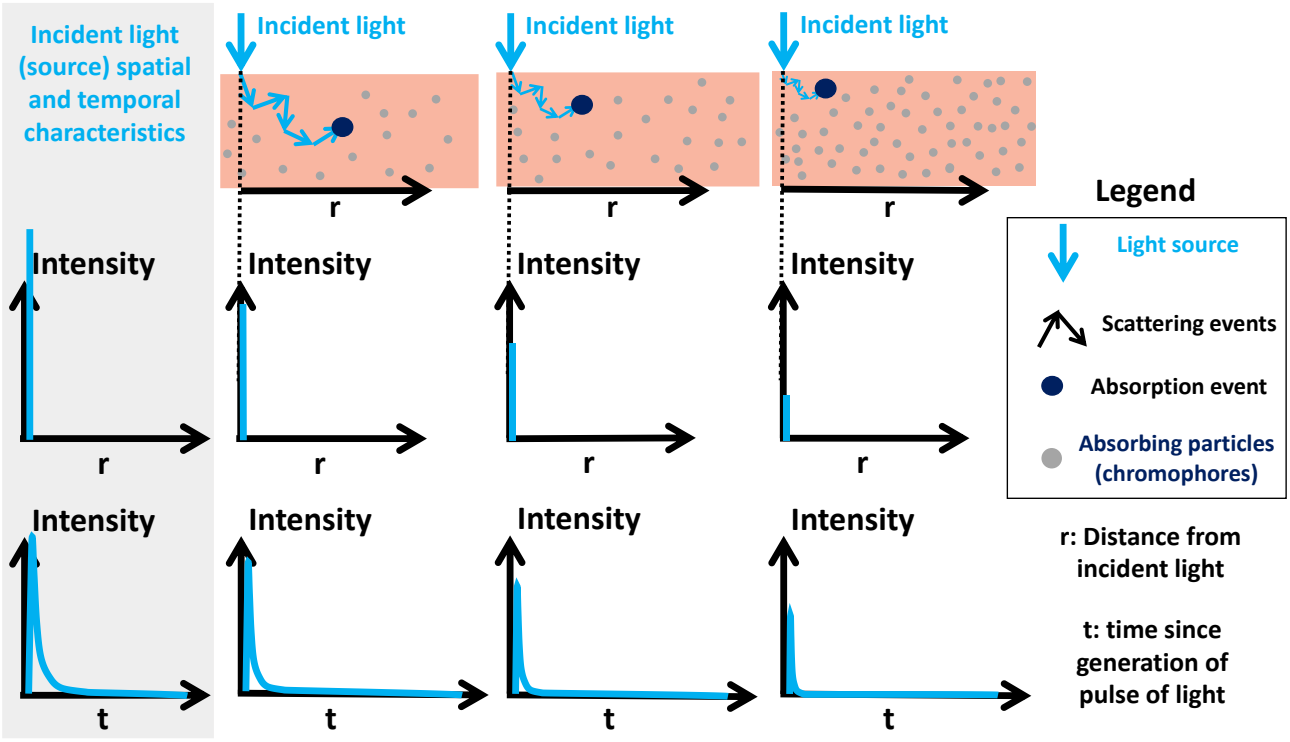


Figure 5.8: Schematic of the relationship between light propagation and diffuse reflected intensity as a function of radial distance r from an infinitesimally narrow light beam (point source) and as a function of time t (for a fixed position in the medium) in an absorbing and single scattering media with increasing μ_a. Schematics of intensity graphs are shown in linear scale. The dashed lines indicate the position of the light source and the distance where most photons were absorbed within the medium.

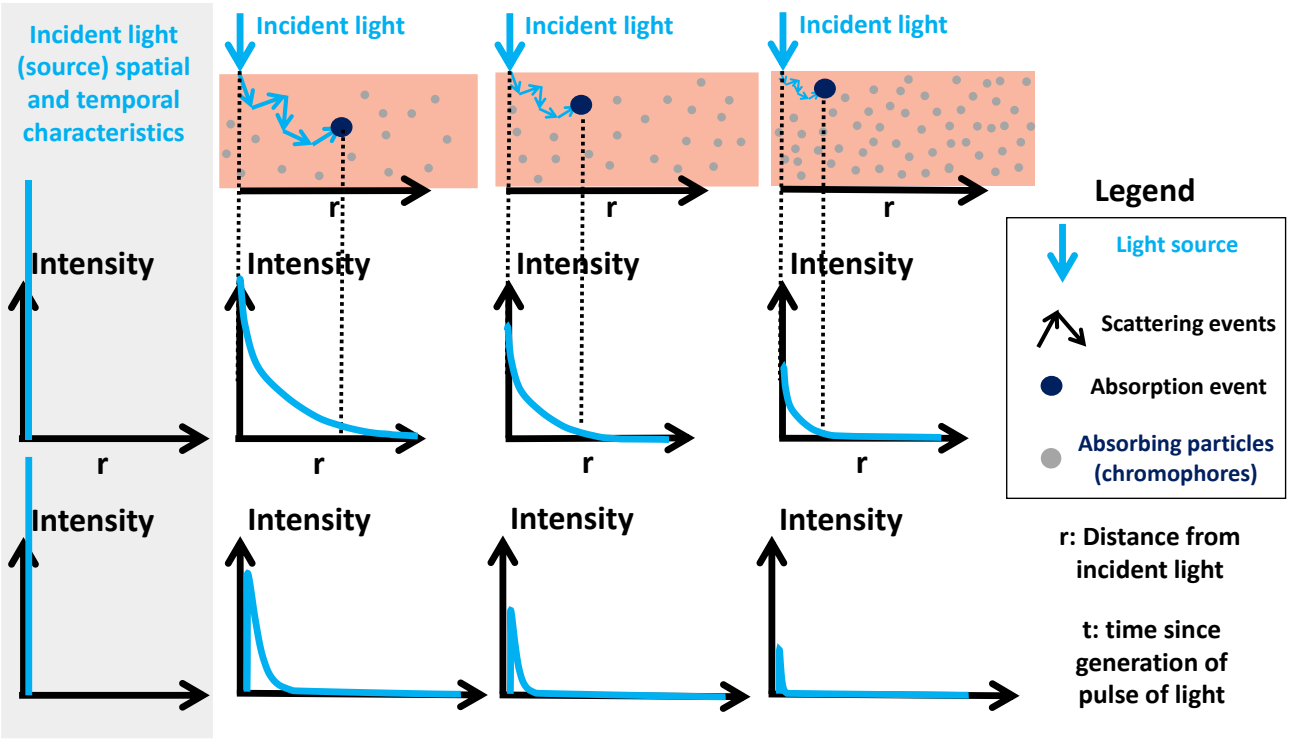


Figure 5.9: Schematic of the relationship between light propagation and diffuse reflected intensity as a function of radial distance r from an infinitesimally narrow light beam (point source) and as a function of time t (for a fixed position in the medium) in an absorbing and multiple scattering media with increasing μ_a. Schematics of intensity graphs are shown in linear scale. The dashed lines indicate the position of the light source and the distance where most photons were absorbed within the medium.

5.3 Luminescence processes

Luminescence processes are analogous to absorption processes. However, where more absorption occurs, more luminescence emission is generated. Therefore, the spatial light distribution due to luminescence follows the same logic as absorption. In a homogenous medium, light is attenuated equally at each medium volume while the remaining light intensity or fluence decreases for larger distances from the light source. Similarly, luminescence is equally generated at each medium volume while excitation light intensity or fluence (responsible to generate luminescence photons) decreases due to absorption. Still, the luminescence light needs to come back to the tissue surface in order to be detected in reflectance or transmittance geometry. Since the luminescence emission is isotropic, photons coming back to the medium surface are not affected by the direction of the incident beam or the distance from the light sources, as opposed to scattering, where high anisotropy factors attenuate the diffuse reflected light due to predominance of forward scattering. The result at reflectance geometry (figure 5.10) is a spatial distribution following the same trend of absorption, i.e., increased luminescence emission close to the light source and an exponential intensity decay as a function of radial distance r. The same rational can be drawn for fluence rates at each depth of the medium. Finally, increased concentration of luminescent particles leads to the following (refer to figure 5.10):

- Higher luminescence emission at all directions within the luminescent medium.
- Higher fluence rates (larger emission) spatially close to the light source.
- The thicker the medium, the higher the transmitted intensity (incidence direction - dashed line) due to higher luminescence generation upon illumination of larger medium volumes.
- The shorter the distance from the light source, the higher the detected luminescence intensity.
- Spatially steeper exponential luminescence intensity decays as a function of distance from the light source.

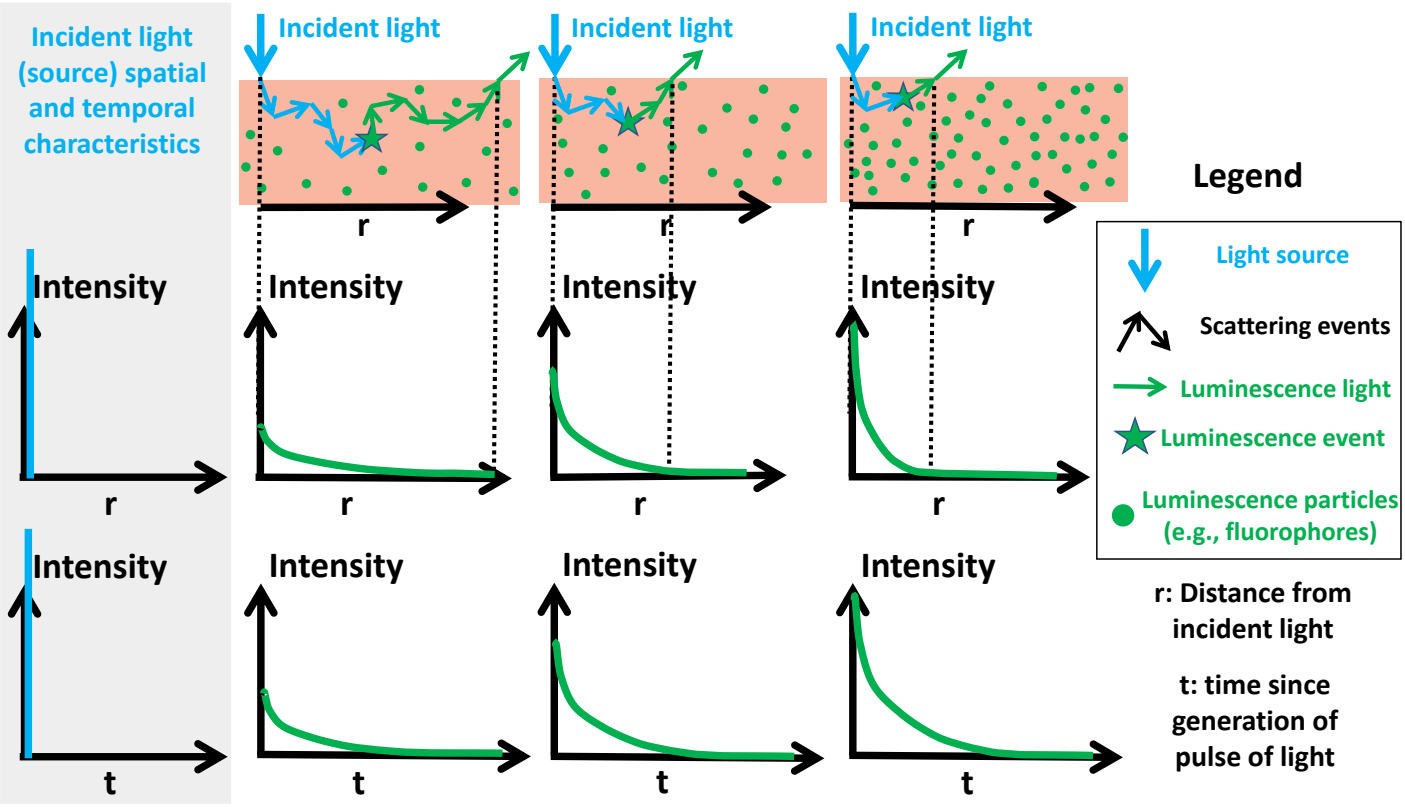


Figure 5.10: Schematic of the relationship between light propagation and luminescence intensity as a function of radial distance r from an infinitesimally narrow light beam (point source) and as a function of time t (for a fixed position in the medium) in a luminescent medium with increasing concentration of luminophores. Schematics of intensity graphs are shown in linear scale. The dashed lines indicate the position of the light source and the distance where most photons exited the luminescent medium.

The analogy between absorption and luminescence processes is valid only for the magnitude (amplitude) of fluorescence over times much longer than the luminescence processes in question. For instance, since fluorescence intensity decays in about 1-100 nanoseconds, the amplitude of average or integrated fluorescence intensity over times in order of milliseconds or longer (as in continuous-wave spectroscopy, chapters 6 and 8, sections 6.3 Time-gating, 8.1.4 Time-resolved (or time-domain) techniques and 8.2.2 Fluorescence spectroscopy (FS)) would follow the opposite trend to absorption as previously described (in luminescence, more absorption leads to more emission). However, the temporal behavior at times shorter than the luminescence decay highly depend on the luminescence lifetime(s) of the sample.

If the luminescent medium has only one luminescence lifetime and is excited by a short pulse of light, the temporal evolution of the luminescence intensity is an exponential decay over time (figure 5.10). Upon increase of the luminophore concentration, the luminescence intensity increases while the exponential decay remains almost unaffected. Since the light typically travels from millimeter to tens of centimeters within biological tissues, increased luminophore concentration may make the luminescence decay a maximum of 3.3 ns sharper (for 100 cm of pathlength). This effect is much less pronounced in biofluids, since their μ_s' is much lower and typical re-emittance cuvette or microfluidic measurements performed either in the magic angle (54.7°) or in 90° ensure that the pathlength difference is between micrometer and a few centimeters (sharpening or broadening of 0.066 ns for a two-centimeter pathlength). Therefore, most of the luminescence intensity variation is dependent on the luminescence lifetime and the only luminescence process which can be affected by the luminophore concentration is the fluorescence process, as fluorescence intensity decays may be in the order of few nanoseconds and phosphorescence decays from 1 millisecond to 10 seconds.

5.4 Convolution of light beams with finite spatial and temporal widths

Real light beams used to illuminate biological media do not have infinitesimal width. Typical light beams are either spatially flat or have spatial Gaussian profiles, whereas the time-domain shape of short light pulses usually resembles a pulse with finite rising time and a fast exponential decay with a narrow width (order of tens to hundreds of picoseconds). In order to calculate the effect due to light beams with finite spatial and temporal widths, it is necessary to convolve the responses of point sources to reconstruct the illumination profile of the light beam used. The general idea of the convolution process is placing a point source at each spatial coordinate and time stamp with non-zero intensity values and summing the effect of all point sources. The power given by each point source is weighted to match the power at each location and time. An illustration of the convolution process for a spatially flat and temporally exponentially-shaped beam to describe the effect on a scattering medium can be seen in the schematic of figure 5.11.

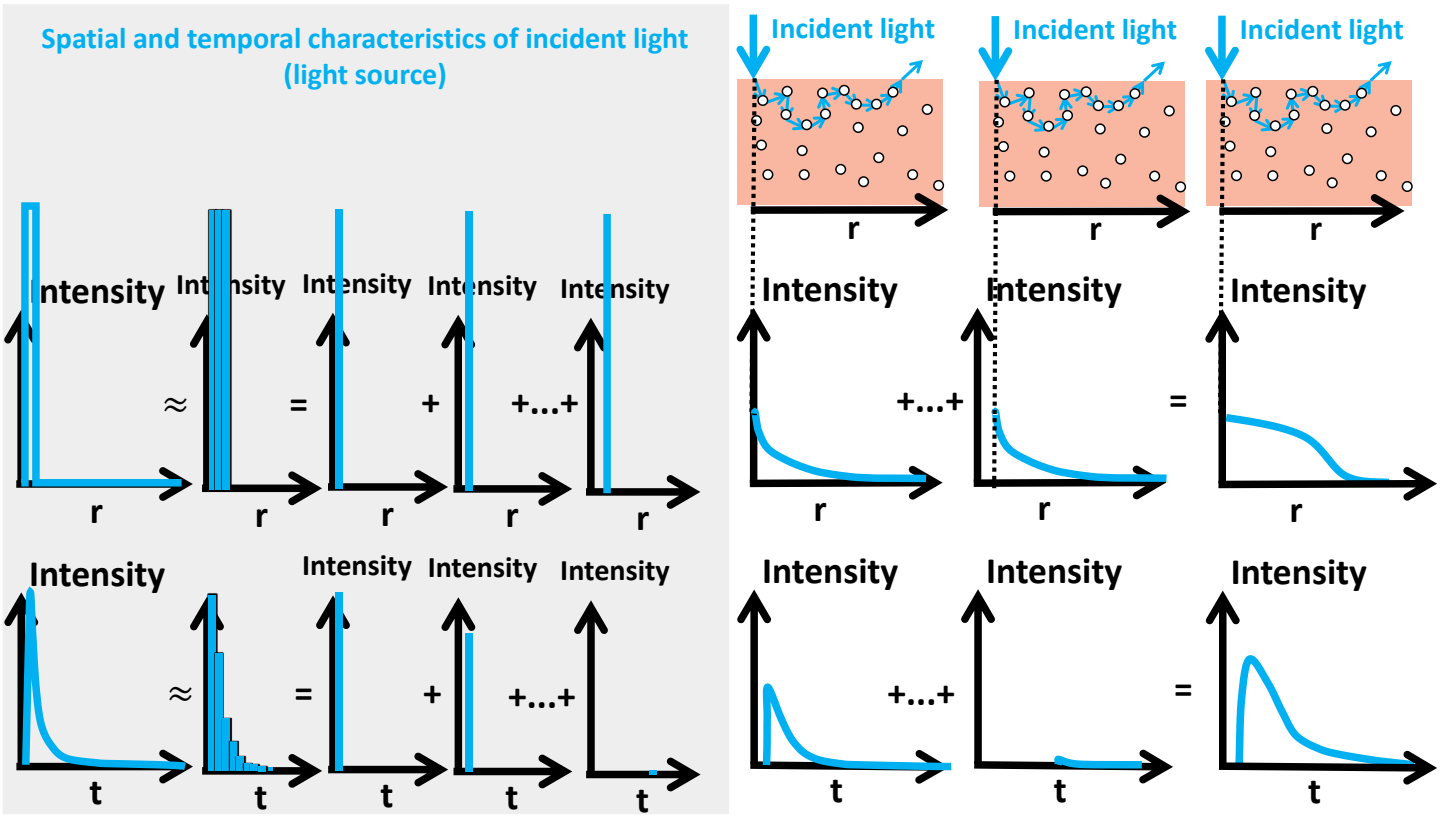


Figure 5.11: Convolution process for calculation of the diffuse reflected intensity of a scattering medium upon illumination by a spatially flat and temporally exponentially-shaped beam.

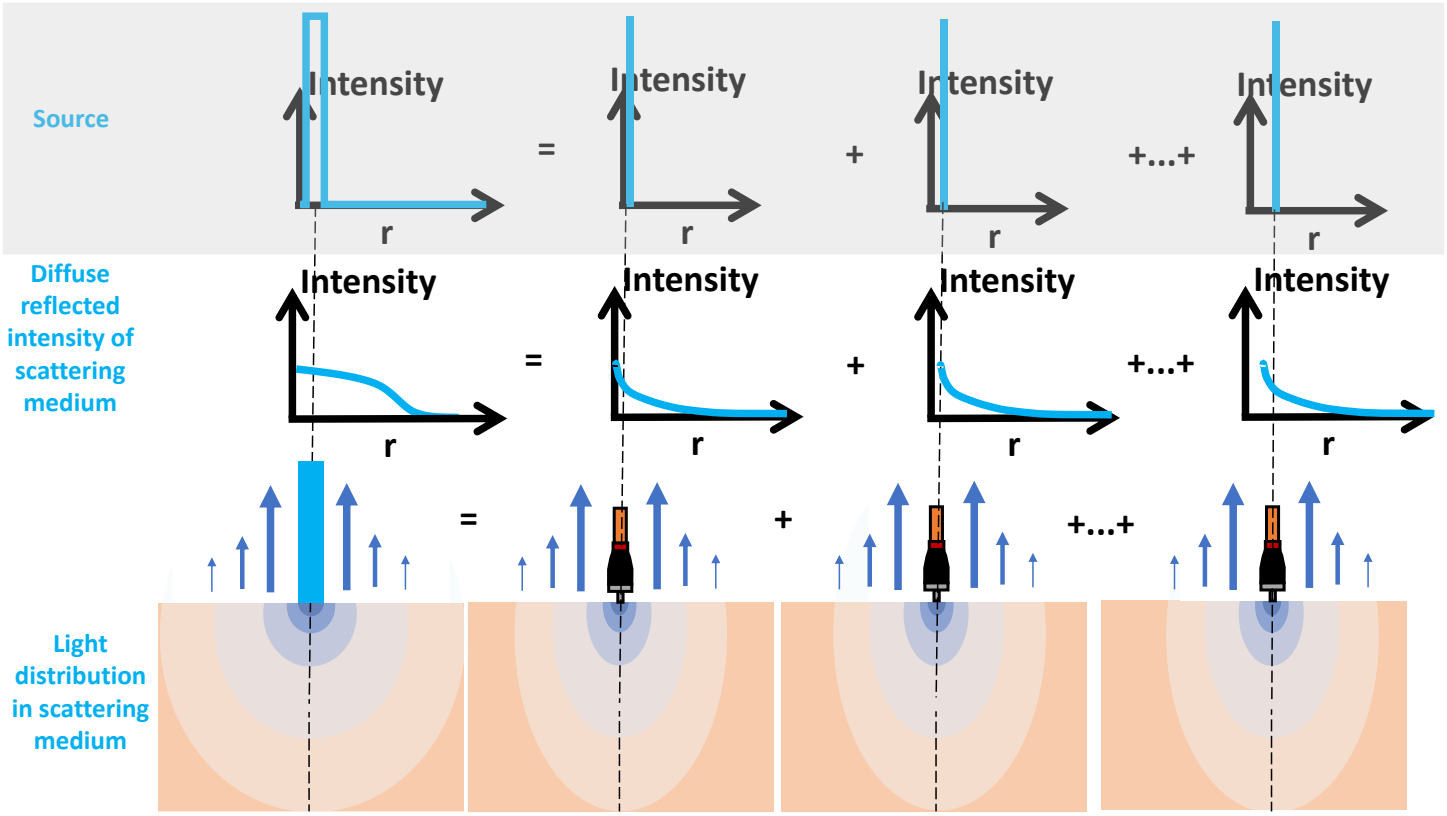


Figure 5.12: Representation of light distribution and the diffuse reflected intensity of a scattering medium illuminated by a spatially flat and temporally exponentially-shaped beam.

Compared to the light propagation when point sources (or infinitesimally narrow beams) are used for illumination, the light distribution in the medium (figure 5.12) happens over a broader area or time period upon illumination using beams with finite spatial and temporal widths (i.e., finite-sized beams). Similarly, the diffuse reflected intensity profiles are broadened in space and time. A similar broadening can be observed in profiles of the transmitted light in slab-shaped media with finite thicknesses. The analogy between the intensity profile in response to illumination by infinitesimally narrow beams and finite-sized beams can be seen by comparing previous schematic drawings of this chapter with figures 5.13, 5.14, 5.15, and 5.16.

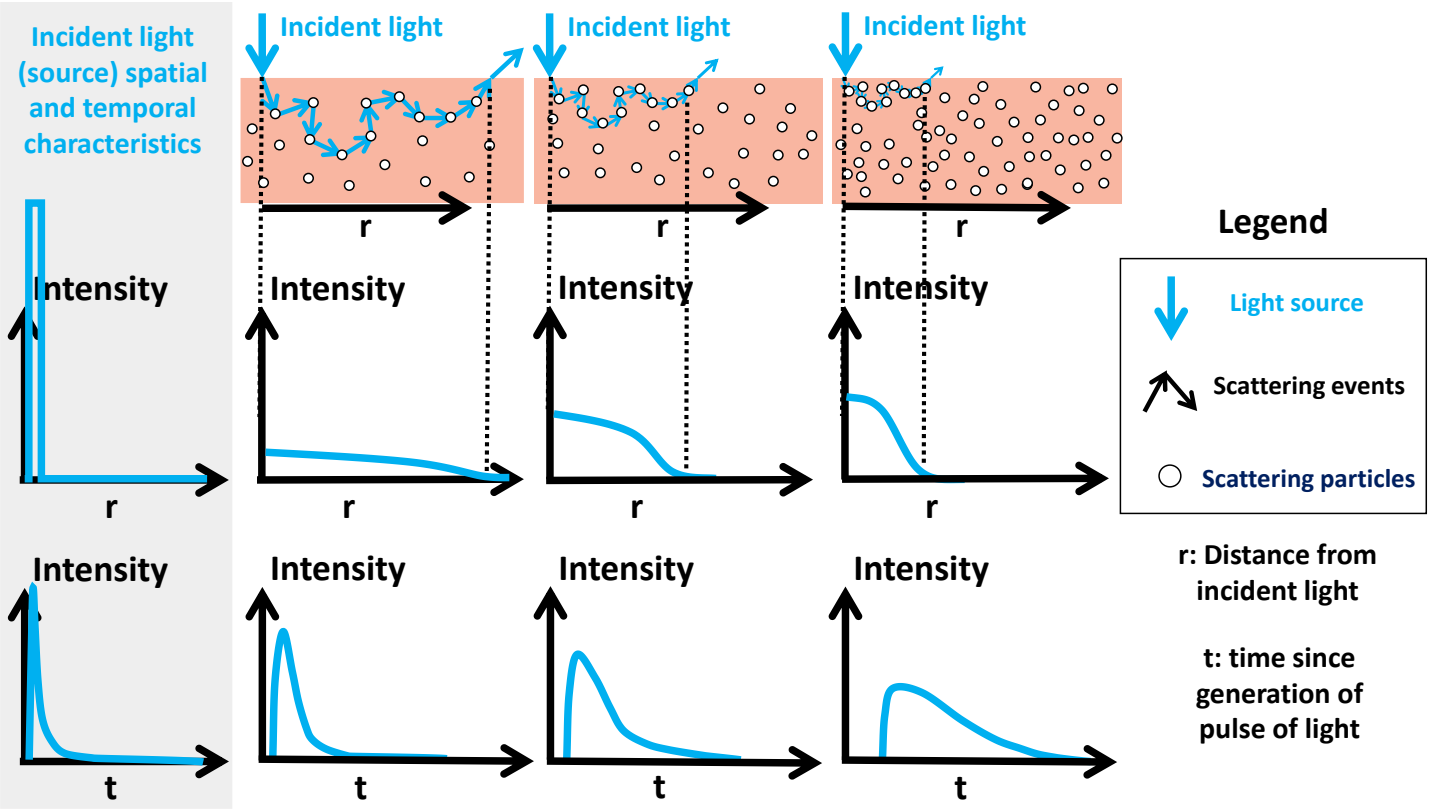


Figure 5.13: Schematic of the relationship between light propagation and diffuse reflected intensity as a function of radial distance r from a finite-sized light beam and as a function of time t (for a fixed position in the medium) in scattering media with increasing μ_s' values. Schematics of intensity graphs are shown in linear scale. The dashed line indicates the distance where most photons exited the scattering medium.

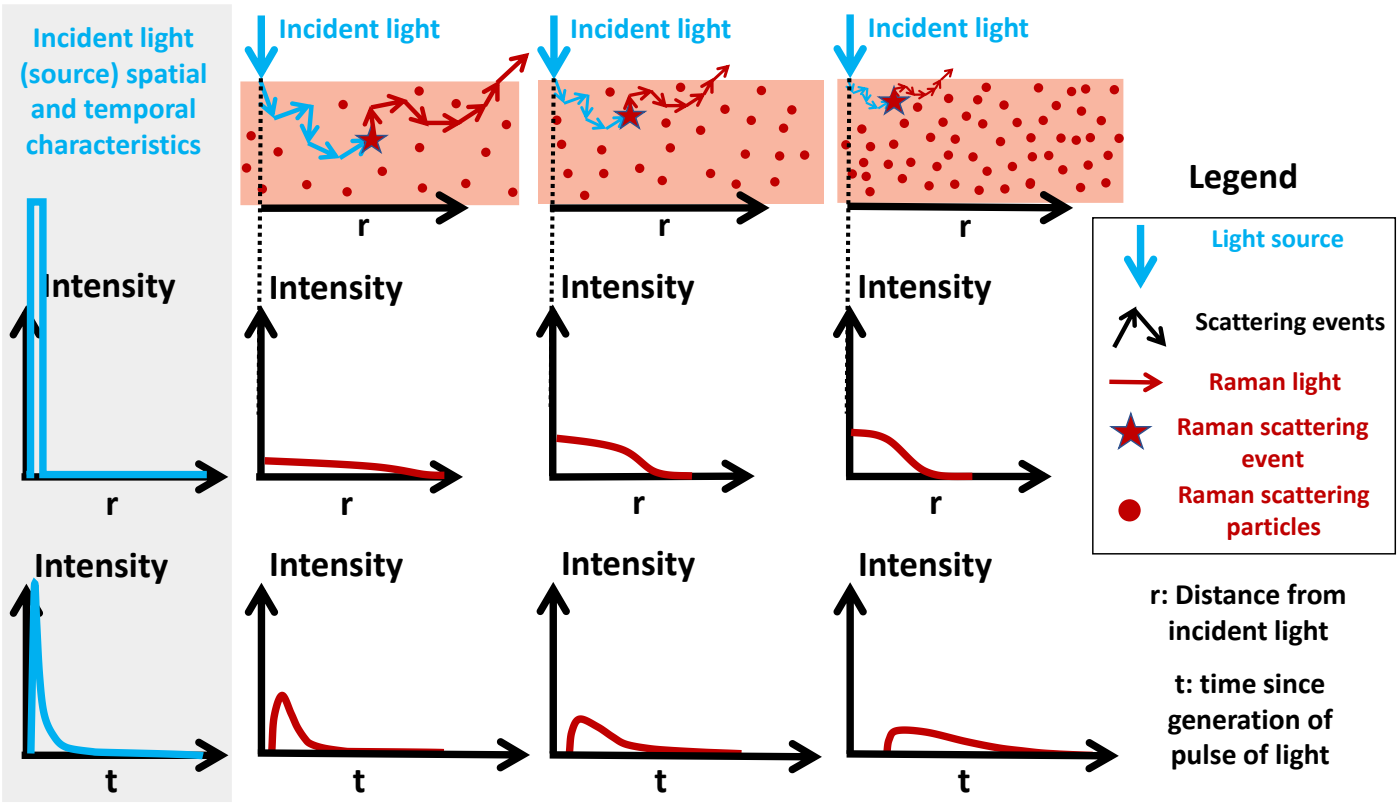


Figure 5.14: Schematic of the relationship between light propagation and diffuse reflected intensity as a function of radial distance r from a finite-sized light beam and as a function of time t (for a fixed position in the medium) in a scattering medium with increasing concentration of Raman scattering particles. Schematics of intensity graphs are shown in linear scale. The shape of intensity profile follows the same trends of that multiple scattering media, but with considerably lower intensity due to the much smaller magnitude of Raman scattering cross-section.

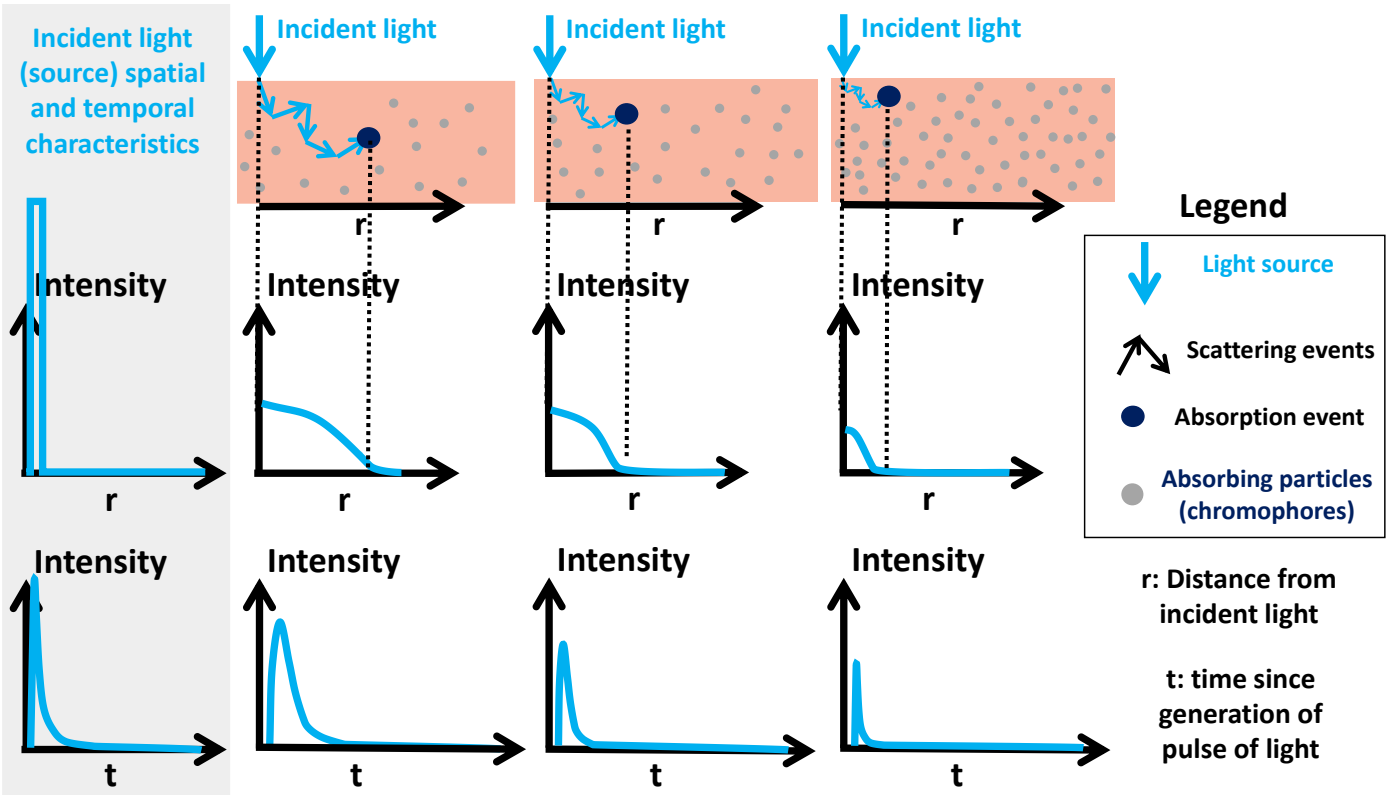


Figure 5.15: Schematic of the relationship between light propagation and diffuse reflected intensity as a function of radial distance r from a finite-sized light beam and as a function of time t (for a fixed position in the medium) in an absorbing and scattering medium with increasing μ_a. Schematics of intensity graphs are shown in linear scale.

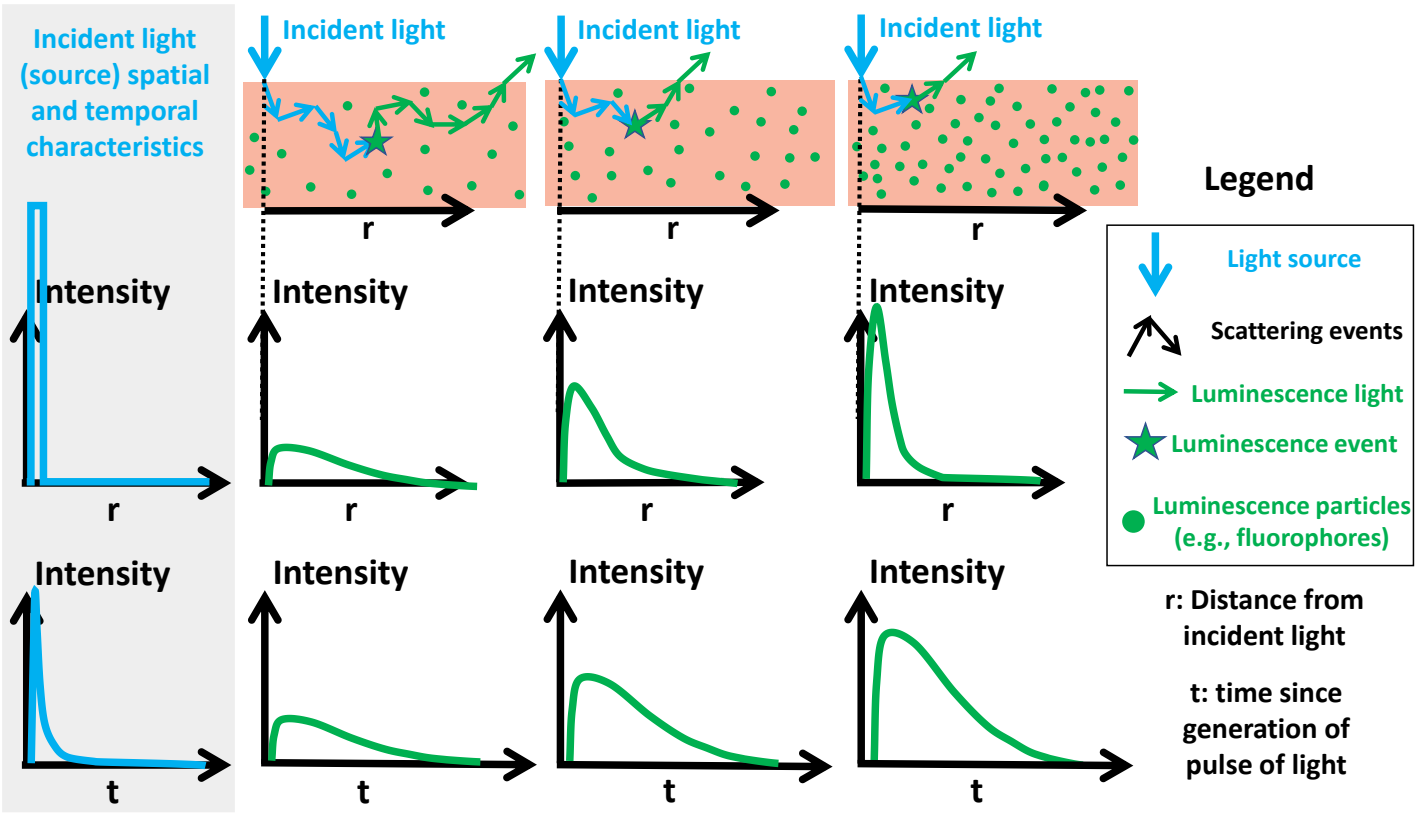


Figure 5.16: Schematic of the relationship between light propagation and luminescence intensity as a function of radial distance r from a finite-sized light beam and as a function of time t (for a fixed position in the medium) in a luminescent medium with increasing concentration of luminophores. Schematics of intensity graphs are shown in linear scale.

5.5 Implications on modeling light behavior in reflectance and transmittance geometries

As described in the previous sections, the spatial and temporal light propagation follows complex patterns which can change considerably depending on the range of the medium optical properties. Examples of cases where this change is pronounced include situations when μ_{Raman} is below or above the limit where multiple Raman scattering should be considered in models of light propagation, as well as those when μ_s' lies in the range where it may cause temporal broadening of the order of fluorescence decays (assuming μ_a is relatively small). The complexity of modeling light propagation may increase if the ranges of optical properties are broad. For instance, light propagation in biological tissues may be difficult to model with only analytical equations due to their wide variation of optical properties as a function of wavelength (μ_s' typically varies between 0.1-100 cm^{-1} while μ_a typically varies between 0.1-1000 cm^{-1} in the visible and near-infrared wavelength ranges [18,19]. This difficulty may increase when considering heterogenous media such as multilayered tissue models with complex medium geometries.

The effect of optical properties in the measured variables also depend on the geometry of illumination and detection (chapter 6, section 6.2). In order to quantitatively and accurately model results of light propagation, several features of this geometry need to be determined such as

- source-to-detector distance (SDD),
- instrument response function (or point spread function in imaging techniques; i.e., spatial and temporal characteristics of the light pulse, sinusoid waveform, continuous illumination),
- detection area,
- angle of illumination and collection (related to numerical aperture of optical fibers),

- contact or non-contact measurements
- reflectance or transmittance geometry

In this chapter the spatial and temporal behavior of diffuse reflected light intensity has been extensively discussed. This behavior is associated with that of re-emitted and transmitted light. In general, the radial and temporal behavior of transmitted light intensity tends to be easier to predict in centimeter-thick biological tissues due to their predominant forward scattering in the visible wavelength range and relatively low light scattering in the infrared range, which means transmittance is typically less affected by photons exiting the surface where light enters the tissue. In addition, realistic transmittance measurements are performed in tissue with centimeters of thickness, where models based on diffusion theory or Beer-lambert law are typically accurate, as long as conditions of the theory underlying each of them is fulfilled (chapter 4, section 4.10.4). Due to the variable geometry and heterogeneity of tissue in the centimeter range, transmittance measurements are mostly used for determination of bulk optical properties.

The current challenge of applications dependent on cost-effective and real-time determination of local tissue optical properties relies on predicting reflectance and re-emittance measurements with limited data available, as these measurements are highly affected by the medium boundaries and determination of boundary conditions typically requires detailed knowledge on the medium geometry (i.e., collection of larger data volumes). Therefore, deducing these measurements at reflectance geometry is necessary to understand the opportunities of the use of state-of-the-art technologies to build new optical instrumentation or of using existing instruments for new applications.

Take home messages

- Chapter 5 connects the physical-mathematical description of light propagation models of chapter 4 with what is experimentally observed in terms of light distribution over biological media (i.e., the source contribution to this distribution). Understanding the temporal and spatial light distribution based on optical properties of biological media such as tissues, biofluids and biosolids is a concept necessary to understand probed depth (one of the main concepts of Papers 1-3 [20,21]), and the behavior of detector measurements (Papers 1-3 [20,21] and publications 6, 7, 9, 10, 16-24 of the "Thesis Output" section [22–32] and publications 3, 4, 7, 11, 13-24, 26, 28-31, and 34-51 [4,5,10,12,33–61] of the "Other publications" section as information on light detection is added in chapter 6 [1–12,20–42,44–46,48–52,55–102].
- The similarity between the behavior of light propagation in absorption and luminescence, and the similarity between light propagation in Raman scattering and Rayleigh scattering processes is important to model signals such as those described in Chapter 17, where fluorescence spectral fitting algorithms have been developed as part of this thesis.
- It is worth noting that Raman scattering is a much weaker optical process compared with Mie scattering and fluorescence processes (μ_{Raman} is typically ~10^{-7} times lower than μ_s' values of biological tissues [13]), which justifies the assumption of $\mu_{Raman} \approx 0$ in spectral fitting algorithms for modeling subdiffuse and diffuse reflectance and for fluorescence signals (Papers 3 and 4 [21,76] (Chapters 14 and 15), and Chapters 17 and 18).

5.6 References

[1] Panhóca, V. H., Nogueira, M. S. and Bagnato, V. S., "Laser and vacuum therapy for treatment of facial nerve palsies," Imaging, Ther. Adv. Technol. Head Neck Surg. Otolaryngol. 2022 **11935**, 39–48 (2022).

[2] Nogueira, M. S., Bagnato, V. S. and Panhoca, V. H., "Effectiveness of whitening treatments employing violet illumination alone or combined with bleaching agents," Proc. SPIE 11942, Photonics West, 11942-6 (2022).

[3] Salvio, A. G., Ramirez, D. P., Inada, N. M., Stringasci, M. D., Nogueira, M. S. and Bagnato, V. S., "Fractionated illumination in a single visit photodynamic therapy for basal cell carcinoma," B. Abstr. (2017).

[4] de Andrade, C. T., Nogueira, M. S., Kanick, S. C., Marra, K., Gunn, J., Andreozzi, J., Samkoe, K. S., Kurachi, C. and Pogue, B. W., "Optical spectroscopy of radiotherapy and photodynamic therapy responses in normal rat skin shows vascular breakdown products," Proc. SPIE 9694 Opt. Methods Tumor Treat. Detect. Mech. Tech. Photodyn. Ther. XXV **9694**, 969410 (2016).

[5] Nogueira, M. S., Brugnera Junior, A., Bagnato, V. S., Panhóca, V. H. and Panhoca, V. H., "Evaluation of the whitening effectiveness of violet illumination alone or combined with hydrogen peroxide gel," Photobiomodulation, Photomedicine, Laser Surg. (2021).

[6] Panhóca, V. H., Nogueira, M. S. and Bagnato, V. S., "Treatment of facial nerve palsies with laser and endermotherapy: a report of two cases," Laser Phys. Lett. **18**(1), 15601 (2020).

[7] Nogueira, M. S., "Ultraviolet-based biophotonic technologies for control and prevention of COVID-19, SARS and related disorders," Photodiagnosis Photodyn. Ther. (2020).

[8] Nogueira, M. S., "Optical theranostics and treatment dosimetry for COVID-19 lung complications: towards increasing the survival rate of vulnerable populations," Photodiagnosis Photodyn. Ther. (2020).

[9] Marcelo, S. N., "Biophotonics for pandemic control: large-area infection monitoring and microbial inactivation of COVID-19," Photodiagnosis Photodyn. Ther. (2020).

[10] Mousavi, M., Moriyama, L. T. T., Grecco, C., Nogueira, M. S., Svanberg, K., Kurachi, C. and Andersson-Engels, S., "Photodynamic therapy dosimetry using multiexcitation multiemission wavelength: toward real-time prediction of treatment outcome," J. Biomed. Opt. **25**(6), 63812 (2020).

[11] Salvio, A. G., Ramirez, D. P., Nogueira, M. S., Stringasci, M. D., Oliveira, E. R., Inada, N. M. and Bagnato, V. S., "Evaluation of pain and treatment effect during large area photodynamic therapy in 140 patients with widespread actinic keratosis of upper limbs," B. Abstr. (2017).

[12] da Silva, A. P., Saito Nogueira, M., Jo, J. A., Salvador Bagnato, V. and Mayumi Inada, N., "Optical Based Diagnosis and Treatment of Onychomycosis," Biomed. Opt. 2016(January), JTu3A.37 (2016).

[13] Reble, C., Gersonde, I. H., Andree, S., Eichler, H.-J. and Helfmann, J., "Quantitative Raman spectroscopy in turbid media," J. Biomed. Opt. **15**(3), 37016 (2010).

[14] Talari, A. C. S., Movasaghi, Z., Rehman, S. and Rehman, I. U., "Raman spectroscopy of biological tissues," Appl. Spectrosc. Rev. **50**(1), 46–111 (2015).

[15] Movasaghi, Z., Rehman, S. and Rehman, I. U., "Raman spectroscopy of biological tissues," Appl. Spectrosc. Rev. **42**(5), 493–541 (2007).

[16] Bhatt, M., Ayyalasomayajula, K. R. and Yalavarthy, P. K., "Generalized Beer--Lambert model for near-infrared light propagation in thick biological tissues," J. Biomed. Opt. **21**(7), 76012 (2016).

[17] Sassaroli, A. and Fantini, S., "Comment on the modified Beer--Lambert law for scattering media," Phys. Med. \& Biol. **49**(14), N255 (2004).

[18] Jacques, S. L., "Optical properties of biological tissues: a review," Phys. Med. Biol. **58**(11), R37 (2013).

[19] Tuchin, V. V and others., "Tissue optics," 2015.

[20] Nogueira, M. S., Maryam, S., Amissah, M., Lu, H., Lynch, N., Killeen, S., O'Riordain, M. and Andersson-Engels, S., "Evaluation of wavelength ranges and tissue depth probed by diffuse reflectance spectroscopy for colorectal cancer detection," Sci. Rep. **11**(1), 1–17 (2021).

[21] Nogueira, M. S., Raju, M., Gunther, J., Maryam, S., Amissah, M., Lu, H., Killeen, S., O'Riordain, M. and Andersson-Engels, S., "Tissue biomolecular and microstructure profiles in optical colorectal cancer delineation," J. Phys. D. Appl. Phys. (2021).

[22] Nogueira, M. S., Matthews, R., Killeen, S., O'Riordain, M. and Andersson-Engels, S., "Colorectal cancer detection based on the extraction of scattering properties and biochemical concentrations from fluorescence spectroscopy measurements," Clin. Transl. Biophotonics, TS2B--5 (2022).

[23] Nogueira, M. S., Raju, M., Gunther, J., Maryam, S., Amissah, M., Lu, H., Killeen, S., O'Riordain, M. and Andersson-Engels, S., "Accurate colorectal cancer detection and delineation by probing superficial and deeper tissue biochemistry and microstructure using diffuse reflectance spectroscopy," Proc. SPIE 11943, Photonics West, 11943-4 (2022).

[24] Nogueira, M. S., Raju, M., Gunther, J., Grygoryev, K., Komolibus, K., Lu, H. and Andersson-Engels, S., "Diffuse reflectance spectroscopy for determination of optical properties and chromophore concentrations of mice internal organs in the range of 350 nm to 1860 nm," Proc. SPIE 10685 Biophotonics Photonic Solut. Better Heal. Care VI **10685**, 106853G (2018).

[25] Nogueira, M. S., Maryam, S., Amissah, M., Lynch, N., Killeen, S., Lu, H., O'Riordain, M. and Andersson-Engels, S., "Improving colorectal cancer detection by extending the near-infrared wavelength range and tissue probed depth of diffuse reflectance spectroscopy: a support vector machine approach," Proc. SPIE 11954, Photonics West, 11954-15 (2022).

[26] Nogueira, M. S., Maryam, S., Amissah, M., Lynch, N., Killeen, S., O'Riordain, M. and Andersson-Engels, S., "Benefit of extending near-infrared wavelength range of diffuse reflectance spectroscopy for colorectal cancer detection using machine learning," Eur. Conf. Biomed. Opt., EW4A--16 (2021).

[27] Nogueira, M. S., Raju, M., Gunther, J., Maryam, S., Amissah, M., Killeen, S., O'Riordain, M. and Andersson-Engels, S., "Optical determination of superficial and deeper tissue biochemistry and microstructure for delineation and early detection of colorectal cancer," Eur. Conf. Biomed. Opt., ETu3A--1 (2021).

[28] Nogueira, M. S., Amissah, M., Maryam, S., Lynch, N., Killeen, S., O'Riordain, M. and Andersson-Engels, S., "Optimization of tissue classification for colorectal cancer detection using support vector machines and diffuse reflectance spectroscopy," Eur. Conf. Biomed. Opt., EW4A--17 (2021).

[29] Nogueira, M. S., Lacerenza, M., Sekar, S. K. V., Buttafava, M., Pifferi, A., Tosi, A., Contini, D. and Andersson-Engels, S., "Broadband extraction of tissue optical properties using a portable hybrid time-resolved continuous wave instrumentation: characterization of ex vivo organs," Clin. Transl. Biophotonics, TM2B--3 (2020).

[30] Lacerenza, M., Pacheco, A., Sekar, S. K. V., Nogueira, M. S., Buttafava, M., Tosi, A., Pifferi, A., Contini, D. and Andersson-Engels, S., "Functional monitoring of lung tissue using a hybrid hyperspectral Time-Resolved GASMAS system: a systematic study on ex vivo sample.," Opt. Tomogr. Spectrosc., SW1D--2 (2020).

[31] Nogueira, M. S., Maryam, S., Amissah, M., Lu, H., Manning, E., Killeen, S., O'Riordain, M. and Andersson-Engels, S., "Broadband diffuse reflectance spectroscopy for colorectal surgical guidance (Conference Presentation)," Opt. Interact. with Tissue Cells XXXI **11238**, 1123802 (2020).

[32] Nogueira, M. S., Komolibus, K., Grygoryev, K., Gunther, J. E. and Andersson-Engels, S., "Fluorescence spectroscopy of mouse organs using ultraviolet excitation: towards assessment of organ viability for transplantation," Proc. SPIE 10876 Opt. Interact. with Tissue Cells XXX **10876**, 1087606 (2019).

[33] e Silva, L. F. das C. and de Carvalho, M. S. N., "Optical techniques for fast screening--towards prevention of the coronavirus COVID-19 outbreak," Photodiagnosis Photodyn. Ther. (2020).

[34] Nogueira, M. S., Bagnato, V. S. and Panhoca, V. H., "Characterization of teeth fluorescence properties due to coffee pigmentation: towards optimization of quantitative light-induced fluorescence for tooth color assessment," Proc. SPIE 11238, Photonics West, 11238-51 (2020).

[35] Nogueira, M. S., Pinto Junior, F. F., Caface, R. A., Oliveira, K. T. de and Guimarães, F. E. G., "Optimization of curcumin formulations for fluorescence-based applications," Proc. SPIE 11238, Photonics West, 11238-50 (2020).

[36] Nogueira, M. S., Bagnato, V. S. and Panhoca, V. H., "Calculation of whiteness and yellowness indexes using

colorimetric and photographic methods for tooth shade evaluation," Proc. SPIE 11238, Photonics West, 11238-52 (2020).

[37] Silami, F. D. J., Pratavieira, S., Nogueira, M. S., Barrett, A. A., Sinhoreti, M. A. C., Geraldeli, S., Pires-de-Souza, F. de C. and others., "Quantitative image of fluorescence of ceramic and resin-cement veneers," Braz. Oral Res. **33** (2019).

[38] Carvalho, L. F. C. S., Nogueira, M. S., Bhattacharjee, T., Neto, L. P. M., Daun, L., Mendes, T. O., Rajasekaran, R., Chagas, M., Martin, A. A. and Soares, L. E. S., "In vivo Raman spectroscopic characteristics of different sites of the oral mucosa in healthy volunteers," Clin. Oral Investig. **23**(7), 3021–3031 (2019).

[39] Carnevalli, A. C., Leal, L., Scherma, A., Morais, C., Martin, F., Bonnier, F., Baker, M., Byrne, H. J., Nogueira, M. S. and others., "Identification of diabetic patients via urine analysis by FTIR: preliminary study (Conference Presentation)," Photonic Diagnosis Treat. Infect. Inflamm. Dis. II **10863**, 108630E (2019).

[40] Nogueira, M. S., Panhóca, V. H. and Bagnato, V. S., "Fluorescence spectroscopy analysis of light-induced tooth whitening," Proc. SPIE 10876, Photonics West, 10876-45 (2019).

[41] Nogueira, M. S., Junior, F. F. P., Caface, R. A., Oliveira, K. T. de, Bagnato, V. S. and Guimarães, F. E. G., "Characterization of photophysical properties of curcumin for theranostics of neurodegenerative diseases," Proc. SPIE 10876, Photonics West, 10876-37 (2019).

[42] Nogueira, M. S., Cosci, A. and Kurachi, C., "Assessment of oxidative stress and metabolic rates in liver grafts using time-resolved fluorescence spectroscopy," Proc. SPIE 10685 Biophotonics Photonic Solut. Better Heal. Care VI **10685**, 106853Z (2018).

[43] Cosci, A., Nogueira, M. S., Pratavieira, S., Takahama, A., Azevedo, R. de S. and Kurachi, C., "Time-resolved fluorescence spectroscopy for clinical diagnosis of actinic cheilitis," Biomed. Opt. Express **7**(10), 4210–4219 (2016).

[44] Cosci, A., Nogueira, M. S., Prataviera, S., Takahama, A., de Souza Azevedo, R. and Kurachi, C., "Time-resolved fluorescence spectroscopy for clinical diagnosis of actinic cheilitis: erratum," Biomed. Opt. Express **9**(2), 648 (2018).

[45] Carvalho, L. F. C. S., Nogueira, M. S., Neto, L. P. M., Bhattacharjee, T. T. and Martin, A. A., "Raman spectral post-processing for oral tissue discrimination – a step for an automatized diagnostic system," Biomed. Opt. Express **8**(11), 5218 (2017).

[46] Carvalho, L. F. C. S., Nogueira, M. S., Neto, L. P. M., Bhattacharjee, T. T. and Martin, A. A., "Raman spectral post-processing for oral tissue discrimination--a step for an automatized diagnostic system: erratum," Biomed. Opt. Express **9**(2), 649 (2018).

[47] Nogueira, M. S., Cosci, A., Rosa, R. G. T., Salvio, A. G., Pratavieira, S. and Kurachi, C., "Portable fluorescence lifetime spectroscopy system for in-situ interrogation of biological tissues," J. Biomed. Opt. **22**(12), 121608 (2017).

[48] Nicolodelli, G., Tadini, A. M., Nogueira, M. S., Pratavieira, S., Mounier, S., Huaman, J. L. C., dos Santos, C. H., Montes, C. R. and Milori, D. M. B. P., "Fluorescence lifetime evaluation of whole soils from the Amazon rainforest," Appl. Opt. **56**(24), 6936–6941 (2017).

[49] Nogueira, M. S., "Fluorescence lifetime spectroscopy for diagnosis of clinically similar skin lesions" (2016).

[50] Nogueira, M. S., Cosci, A., Pratavieira, S., Takahama Jr, A., Azevedo, R. S. and Kurachi, C., "Evaluation of actinic cheilitis using fluorescence lifetime spectroscopy," Proc. SPIE 9703 Opt. Biopsy XIV Towar. Real-Time Spectrosc. Imaging Diagnosis **9703**, 97031U (2016).

[51] Nogueira, M. S. and Kurachi, C., "Assessing the photoaging process at sun exposed and non-exposed skin using fluorescence lifetime spectroscopy," Proc. SPIE 9703 Opt. Biopsy XIV Towar. Real-Time Spectrosc. Imaging Diagnosis **9703**, 97031W (2016).

[52] Nogueira, M. S., Rosa, R. G. T., Pratavieira, S., de Paula, D. and Kurachi, C., "Assembly and characterization of a fluorescence lifetime spectroscopy system for skin lesions diagnostic," Proc. SPIE 9531 Biophotonics South Am.

9531, 95313D (2015).

[53] Almeida, C. D. P. D., Campos, C., Nogueira, M. S. and Kurachi, C., "Time-resolved and steady-state fluorescence spectroscopy for the assessment of skin photoaging process," Proc. SPIE 9531, Biophotonics South Am. 953146 (June 19, 2015) **9531**(June 2015), 1–7 (2015).

[54] Pires, L., Nogueira, M. S., Pratavieira, S., Moriyama, L. T. and Kurachi, C., "Time-resolved fluorescence lifetime for cutaneous melanoma detection," Biomed. Opt. Express **5**(9), 3080 (2014).

[55] Kurachi, C., Pires, L., Nogueira, M. S. and Pratavieira, S., "Lifetime fluorescence for the detection of skin lesions," Biomed. Opt. 2014(April), BS4B.3 (2014).

[56] Ferreira, M. C. de M. S. C., Leal, L. B., Nogueira, M. S., Castro, P. A. A., Peralta, F., Zezell, D. M. and Carvalho, L. F. C. S., "Biochemical characterization of saliva of smoking and non-smoking patients by using Fourier-transform infrared spectroscopy," Proc. SPIE 11957, Photonics West, 11957-49 (2022).

[57] Nogueira, M. S., Leal, L. B., Marcarini, W. D., Pimentel, R. L., Muller, M., Vassallo, P. F., Campos, L. C. G., Dos Santos, L., Luiz, W. B., Mill, J. G. and others., "Rapid diagnosis of COVID-19 using FT-IR ATR spectroscopy and machine learning," Sci. Rep. **11**(1), 1–13 (2021).

[58] Nogueira, M. S., Leal, L. B., Marcarini, W. D., Pimentel, R. L., Muller, M., Vassallo, P. F., Campos, L. C. G., Dos Santos, L., Luiz, W. B., Mill, J. G. and others., "Author Correction: Rapid diagnosis of COVID-19 using FT-IR ATR spectroscopy and machine learning," Sci. Rep. **11**(1), 1 (2021).

[59] Saito Nogueira, M., Ribeiro, V., Pires, M., Peralta, F. and others., "Biochemical Profiles of In Vivo Oral Mucosa by Using a Portable Raman Spectroscopy System," Optics **2**(3), 134–147 (2021).

[60] Leal, L. B., Nogueira, M. S., Mageski, J. G. A., Martini, T. P., Barauna, V. G., Dos Santos, L., e Silva, L. F. das C. and others., "Diagnosis of Systemic Diseases Using Infrared Spectroscopy: Detection of Iron Overload in Plasma—Preliminary Study," Biol. Trace Elem. Res., 1–15.

[61] Nogueira, M. S., "Biophotonic telemedicine for disease diagnosis and monitoring during pandemics: overcoming COVID-19 and shaping the future of healthcare," Photodiagnosis Photodyn. Ther. (2020).

[62] Bunaciu, A. A., Hoang, V. D. and Aboul-Enein, H. Y., "Applications of FT-IR spectrophotometry in cancer diagnostics," Crit. Rev. Anal. Chem. **45**(2), 156–165 (2015).

[63] Leal, L. B., Nogueira, M. S., Canevari, R. A. and Carvalho, L., "Vibration spectroscopy and body biofluids: Literature review for clinical applications," Photodiagnosis Photodyn. Ther. (2018).

[64] Cosci, A., Nogueira, M. S., Pratavieira, S., Takahama, A., Azevedo, R. de S., Kurachi, C. and Kurachi, C., "Time-resolved fluorescence spectroscopy for clinical diagnosis of actinic cheilitis," Biomed. Opt. Express **7**(10), 4210–4219 (2016).

[65] de Paula, D., Campos, C., Nogueira, M. S., Pratavieira, S. and Kurachi, C., "Time-resolved and steady-state fluorescence spectroscopy for the assessment of skin photoaging process," Proc. SPIE 9531 Biophotonics South Am. **9531**, 953146 (2015).

[66] Nogueira, M. S. and Guimarães, F. E. G., "Photophysical processes on biological tissues and photodynamic therapy using steady-state and time-resolved fluorescence techniques: diagnosis applications, dosimetry and photodegradation kinetics," Livro de Resumos (2016).

[67] de Paula Campos, C., de Paula D'Almeida, C., Nogueira, M. S., Moriyama, L. T., Pratavieira, S. and Kurachi, C., "Fluorescence spectroscopy in the visible range for the assessment of UVB radiation effects in hairless mice skin," Photodiagnosis Photodyn. Ther. **20**(May), 21–27 (2017).

[68] Nogueira, M. S., D'Almeida, C. P., Pratavieira, S. and Kurachi, C., "Characterization of a fluorescence lifetime spectroscopy system for diagnostic purposes using an optic fiber probe," Livro de Resumos (2014).

[69] Pires, L., Nogueira, M. S., Moriyama, L. T. and Kurachi, C., “Fluorescence lifetime for melanoma murine detection,” Tech. Summ. (2014).

[70] Nogueira, M., D’Almeida, C. P., Cosci, A., Pratavieira, S., Kurachi, C. and Schimdt, P. A., “Montagem e caracterização de sistema de espectroscopia e tempo de vida de fluorescência utilizando fibra óptica,” XXIV Congr. Bras. Eng. Biomédica--CBEB. Uberlandia, 2468–2471 (2014).

[71] Nogueira, M. S., D’Almeida, C. P., Pratavieira, S. and Kurachi, C., “Sistema de espectroscopia e tempo de vida de fluorescência para diagnóstico clinico,” Anais/Resumos (2015).

[72] Nogueira, M. S., Pratavieira, S., Kurachi, C. and others., “Portable fluorescence microendoscope system for smartphones and imaging processing software,” Tech. Summ. (2015).

[73] Ono, B. A., Nogueira, M., Pires, L., Pratavieira, S. and Kurachi, C., “Subcellular localization and photodynamic activity of Photodithazine (glucosamine salt of chlorin e6) in murine melanoma B16-F10: an in vitro and in vivo study,” Proc. SPIE 10476 Opt. Methods Tumor Treat. Detect. Mech. Tech. Photodyn. Ther. XXVII **10476**(February), 44 (2018).

[74] Nogueira, M. S., Pratavieira, S., Júnior, A. T., Azevedo, R. S. and Kurachi, C., “Diagnóstico de queilite actinica por espectroscopia de tempo de vida de fluorescência,” Anais/Resumos (2015).

[75] Pires, L., Nogueira, M. S., Pratavieira, S., Moriyama, L. T. and Kurachi, C., “Time-resolved fluorescence lifetime for cutaneous melanoma detection,” Biomed. Opt. Express **5**(9), 3080 (2014).

[76] Nogueira, M. S., Raju, M., Komolibus, K., Grygoryev, K. and Andersson-Engels, S., “Assessment of tissue biochemical and optical scattering changes due to hypothermic organ preservation: a preliminary study in mouse organs,” J. Phys. D. Appl. Phys. (2021).

[77] Nogueira, M. S., Gunther, J. E., Komolibus, K. and Andersson-Engels, S., “User-friendly graphical user interface for simulating tissue optical properties and fluence rates: improving students learning in tissue optics,” Opt. Interact. with Tissue Cells XXXI **11238**, 112380B (2020).

[78] Nogueira, M. S., Gunther, J. E., Komolibus, K., Ryan, S. M., Murray, B., Jezzini, M. A., Kennedy, D. and Andersson-Engels, S., “Method of continuous improvement of multidisciplinary programs and outreach activities,” Educ. Train. Opt. Photonics, 11143_41 (2019).

[79] Nogueira, M. S., Gunther, J., Komolibus, K. and Andersson-Engels, S., “Teaching light-tissue interactions: using technology for education,” Opt. Interact. with Tissue Cells XXX **10876**, 108761H (2019).

[80] Nogueira, M. S., Komolibus, K., Tobo, A. L. P., Jayet, B., Sekar, S. K. V., Sorensen, S., Tyndall, C. and Andersson-Engels, S., “Biophotonics box: educational kit for multidisciplinary outreach activities in optics and photonics,” Educ. Train. Opt. Photonics, W4B--5 (2021).

[81] “BIOPHOTONICS BOX | Marcelo Saito Nogueira | Research Project.”, <https://www.researchgate.net/project/Biophotonics-box> (2 November 2021).

[82] Nogueira, M. S., Komolibus, K., Gunther, J. E., Sekar, S. K. V., Jayet, B., Tobo, A. L. P., Li, C. L., Maryam, S., Tyndall, C., Kennedy, D. and others., “Online learning combining virtual lectures, at-home experiments and computer simulations: a multidisciplinary teaching and learning approach,” Educ. Train. Opt. Photonics, F2B--6 (2021).

[83] Saito Nogueira, M., Gunther, J. E., Jayet, B., Souza Matias, J., Tyndall, C. and Andersson-Engels, S., “Biophotonics computer app: fostering multidisciplinary distance self-paced learning with a user-friendly interface,” OSA Tech. Dig., 1–2 (2021).

[84] Nogueira, M. S., “Espectroscopia de tempo de vida de fluorescência para o diagnóstico de lesões de pele clinicamente semelhantes” (2016).

[85] Panhoca, V. H., Nogueira, M. S. and Bagnato, V. S., “Laser and vacuum therapy for treatment of facial nerve palsies,” Proc. SPIE 11935, Photonics West, 11935-21 (2022).

[86] Nogueira, M. S., Jayet, B., Matias, J. S., Gunther, J. E., Tyndall, C. and Andersson-Engels, S., "Biophotonics web application for computer simulations in diffuse optics: fostering multidisciplinary education and research," Proc. SPIE 11958, Photonics West, 11958-18 (2022).

[87] Nogueira, M. S., Li, C. L., Maryam, S., Tyndall, C., Donovan, S., Komolibus, K., Gunther, J. E., Sekar, S. K. V., Jayet, B., Fisher, C., Kennedy, D. and Andersson-Engels, S., "Multidisciplinary teaching and learning biophotonics: assessing the effectiveness of fully online outreach events," Proc. SPIE 11958, Photonics West, 11958-39 (2022).

[88] e Silva, L. F. das C., Nogueira, M. S. and others., "New insights of Raman spectroscopy for oral clinical applications," Analyst **143**(24), 6037–6048 (2018).

[89] Carvalho, L. F. C. S., Nogueira, M. S., Bhattacharjee, T., Neto, L. P. M., Daun, L., Mendes, T. O., Rajasekaran, R., Chagas, M., Martin, A. A. and Soares, L. E. S., "In vivo Raman spectroscopic characteristics of different sites of the oral mucosa in healthy volunteers," Clin. Oral Investig., 1–11 (2018).

[90] Nogueira, M. S., Barreto, A. L., Furukawa, M., Rovai, E. S., Bastos, A., Bertoncello, G., e Silva, L. F. das C. and others., "FTIR spectroscopy as a point of care diagnostic tool for diabetes and periodontitis: A saliva analysis approach," Photodiagnosis Photodyn. Ther. **40**, 103036 (2022).

[91] Nogueira, M. S., Brugnera Junior, A., Bagnato, V. S. and Panhóca, V. H., "Evaluation of the whitening effectiveness of violet illumination alone or combined with hydrogen peroxide gel," Photobiomodulation, Photomedicine, Laser Surg. (2021).

[92] Nogueira, M. S., "Biophotonics for pandemic control: large-area infection monitoring and microbial inactivation of COVID-19," Photodiagnosis Photodyn. Ther. **31**, 101823 (2020).

[93] Carvalho, L. F. das C. e S. and Saito Nogueira, M., "Optical techniques for fast screening--towards prevention of the coronavirus COVID-19 outbreak," Photodiagnosis Photodyn. Ther. (2020).

[94] Ferreira, M. C. C., Monteiro, G. R., Peralta, F., Castro, P. A. A., Zezell, D., Nogueira, M. S. and Carvalho, L. F. C. S., "Assessment of bound water of saliva samples by using FT-IR spectroscopy," Lat. Am. Opt. Photonics Conf., M4B--1 (2022).

[95] Bomfin, L. S., Kitakawa, D., Nogueira, M. S., e Silva, L. F. das C. and others., "Low Level Laser Therapy as adjuvant treatment for lower lip lesion," Lat. Am. Opt. Photonics Conf., M2B--6 (2022).

[96] Maryam, S., Nogueira, M. S., Krishnamoorthy, S., Sekar, S. K. V., Lu, H., Gautam, R., Burke, R., Andersson-Engels, S., Riordain, R. N. and Sheahan, P., "Multi-configuration Raman spectrometer for early stage diagnosis of oral cancer," Biomed. Vib. Spectrosc. 2022 Adv. Res. Ind. **11957**, 20–26 (2022).

[97] Maryam, S., Sekar, S. K. V., Gautam, R., Kho, K. W., Ghauri, D., Nogueira, M. S., Beffara, F., Fahy, E., Riordain, R. N., Burke, R., Sheahan, P., Feeley, L. and Andersson-Engels, S., "Portable multi-configuration clinical translational Raman system for oral cancer application," Analyst (2022).

[98] Nogueira, M. S., Ferreira, M. C. M. S. C., Leal, L. B., Castro, P. A. A., Peralta, F., Zezell, D. M. and Carvalho, L. F. C. S., "A validation step for point of care diagnostics through saliva characterization of smoking patients by using FTIR spectroscopy," Exp. Mol. Pathol. (2023).

[99] Coelho, M. C. M. S., Leal, L. B., Nogueira, M. S., Castro, P. A. A., Peralta, F., Zezell, D. M. and others., "Biochemical characterization of saliva of smoking and non-smoking patients by using Fourier-transform infrared spectroscopy," Biomed. Vib. Spectrosc. 2022 Adv. Res. Ind. **11957**, 86–97 (2022).

[100] Saito Nogueira, M., Maryam, S., Amissah, M., McGuire, A., Spillane, C., Killeen, S., Andersson-Engels, S. and O'Riordain, M., "Insights into Biochemical Sources and Diffuse Reflectance Spectral Features for Colorectal Cancer Detection and Localization," Cancers (Basel). **14**(22), 5715 (2022).

[101] Panhóca, V. H., Nogueira, M. S., Zanin, F. A. A., Brugnera, A. P., Brugnera Jr, A. and Bagnato, V. S., "Dental sensitivity and color change in patients undergoing dental bleaching with application of violet light," Oral Health Dent. Manag.

21(6), 1–14 (2022).

[102] Panhóca, V. H., Aquino Junior, A. E., Souza, V. B., Ferreira, S. A., Ferreira, L. T., Souza, K. J. O., Tamae, P. E., Saito Nogueira, M. and Bagnato, V. S., “Effects of red and infrared laser therapy in patients with tinnitus: a double-blind, clinical, randomized controlled study combining light with ultrasound, drugs and vacuum therapy,” J. Pers. Med. (2023).